Age-specific function of alpha 5 beta 1 integrin in microglial migration during early colonization of the developing mouse cortex

Peer-reviewed author version

SMOLDERS, Sophie; SWINNEN, Nina; KESSELS, Sofie; Arnauts, Kaline; SMOLDERS, Silke; Le Bras, Barbara; RIGO, Jean-Michel; Legendre, Pascal & BRONE, Bert (2017) Age-specific function of alpha 5 beta 1 integrin in microglial migration during early colonization of the developing mouse cortex. In: GLIA (New York, N.Y. : Print), 65(7), p. 1072-1088.

DOI: 10.1002/glia.23145
Handle: http://hdl.handle.net/1942/23955

Age-specific function of α5β1 integrin in microglial migration during early colonization of the developing mouse cortex

Journal:	*GLIA*
Manuscript ID	GLIA-00447-2016.R1
Wiley - Manuscript type:	Original Research Article
Date Submitted by the Author:	n/a
Complete List of Authors:	Smolders, Sophie; UHasselt, BIOMED; INSERM, UMR-S 1130, CNRS, UMR 8246, Neuroscience Paris Seine, Institute of Biology Paris Seine; Sorbonne Universités, UPMC Université Paris 06, UM CR18, Neuroscience Paris Seine Swinnen, Nina; UHasselt, BIOMED Kessels, Sofie; UHasselt, BIOMED Arnauts, Kaline; UHasselt, BIOMED Smolders, Silke; UHasselt, BIOMED; KU Leuven, Laboratory of Neuronal Differentiation, VIB Center for the Biology of Disease, Leuven and Center for Human Genetics Le Bras, Barbara; INSERM, UMR-S 1130, CNRS, UMR 8246, Neuroscience Paris Seine, Institute of Biology Paris Seine; Sorbonne Universités, UPMC Université Paris 06, UM CR18, Neuroscience Paris Seine Rigo, Jean-Michel; UHasselt Legendre, Pascal; INSERM, UMR-S 1130, CNRS, UMR 8246, Neuroscience Paris Seine, Institute of Biology Paris Seine; Sorbonne Universités, UPMC Université Paris 06, UM CR18, Neuroscience Paris Seine Brône, Bert; UHasselt, BIOMED
Key Words:	Embryo, Cell Adhesion Molecules, Fibronectins, Cell Migration Inhibition, Blood Vessels

Note: The following files were submitted by the author for peer review, but cannot be converted to PDF. You must view these files (e.g. movies) online.

Smolders_Suppl_Movie 1.avi
Smolders_Suppl_Movie 2.avi
Smolders_Suppl_Movie 3.avi
Smolders_Suppl_Movie 4.avi
Smolders_Suppl_Movie 5.avi
Smolders_Suppl_Movie 6.avi
Smolders_Suppl_Movie 7.avi
Smolders_Suppl_Movie 8.avi

1) Title page

Age-specific function of α5β1 integrin in microglial migration during early colonization of the developing mouse cortex

Sophie Marie-Thérèse Smolders [1,2,3], Nina Swinnen [1], Sofie Kessels [1], Kaline Arnauts [1], Silke Smolders [1,4], Barbara Le Bras [2,3], Jean-Michel Rigo [5], Pascal Legendre [2,3]*, Bert Brône [1]*

[1] UHasselt, BIOMED Research Institute, Diepenbeek, Belgium
[2] INSERM, UMR-S 1130, CNRS, UMR 8246, Neuroscience Paris Seine, Institute of Biology Paris Seine, Paris, France
[3] Sorbonne Universités, UPMC Université Paris 06, UM CR18, Neuroscience Paris Seine, Paris, France
[4] Laboratory of Neuronal Differentiation, VIB Center for the Biology of Disease, Leuven and Center for Human Genetics, KU Leuven, Leuven, Belgium
[5] UHasselt, Campus Hasselt, Belgium

* equally contributing

Mailing adresses

Sophie.smolders@uhasselt.be, Nina.swinnen@gmail.com, Sofie.Kessels@uhasselt.be, Kaline.arnauts@gmail.com, Silke.smolders@uhasselt.be, Barbara.cailbourdin@upmc.fr, Jeanmichel.rigo@uhasselt.be, Pascal.legendre@inserm.fr, Bert.brone@uhasselt.be

Running title not to exceed 45 letters and spaces

Count: 42
Migration of microglia in the mouse embryo

The exact number of words (by section, including legends and bibliography), figures and tables in the article, plus the total word count

Word count total: 12077
1) Title page: 300
2) Abstract: 184
3) Text total: 7617
    Introduction: 667
    Materials & Methods: 2343
    Results: 2478
    Discussion: 2129
4) Acknowledgements:140
5) References: 2009 (#78)
6) Figure legends: 1816
7) Figures: 6 + 1 Suppl. Fig
8) Tables: 0

Individual, address, and telephone number to whom correspondence concerning manuscript should be sent.

Bert Brône
Martelarenlaan 42, 3500 Hasselt
Belgium
+32 11 26 92 37

Pascal Legendre
Batiment B, etage 2, boite postale 37
7 quai Saint Bernard
75005 Paris
France
+33 1 44 27 91 63

Main Points

Count: 217

1) α5β1 integrin regulates the migration of microglia during embryonic corticogenesis
2) A developmental switch of α5β1 integrin function occurs between E13.5 and E15.5 from promoting to inhibiting microglial migration

Table of Contents Image (TOCI)

see separate figure upload

Key Words

Count: 79

Embryo - Blood Vessels - Cell Adhesion Molecules - Fibronectins - Cell Migration Inhibition

2) Abstract

Microglia, the immune cells of the central nervous system, take part in brain development and homeostasis. They derive from primitive myeloid progenitors that originate in the yolk sac and colonize the brain mainly through intensive migration. During development, microglial migration speed declines which suggests that their interaction with the microenvironment changes. However, the matrix-cell interactions allowing dispersion within the parenchyma are unknown. Therefore, we aimed to better characterize the migration behavior and to assess the role of matrix-integrin interactions during microglial migration in the embryonic brain *ex vivo*. We focused on microglia-fibronectin interactions mediated through the fibronectin receptor α5β1 integrin because *in vitro* work indirectly suggested a role for this ligand-receptor pair. Using 2-photon time-lapse microscopy on acute *ex vivo* embryonic brain slices, we found that migration occurs in a saltatory pattern and is developmentally regulated. Most importantly, there is an age-specific function of the α5β1 integrin during microglial cortex colonization. At embryonic day (E)13.5, α5β1 facilitates migration while as from E15.5, it inhibits migration. These results indicate a developmentally regulated function of α5β1 integrin in microglial migration during colonization of the embryonic brain.

3) Text

INTRODUCTION

Microglia, the immune cells of the central nervous system (CNS), are renowned as the first line defense during brain disease. The last decade researchers have been exploring the plentiful non-immunological tasks of these cells and found them to be involved in normal brain development and homeostasis, through influencing neurogenesis, axonal growth, synapse refinement, blood vessel branching and clearance of dying neurons (Casano and Peri 2015; Frost and Schafer 2016). Microglial cells originate from primitive myeloid progenitor cells that arise from the yolk sac at embryonic day (E) 7.5 in mice. Primitive macrophages migrate to the CNS using the blood circulation and adopt a microglia phenotype when they invade the brain and spinal cord parenchyma around E10.5 and E11.5, respectively (Ginhoux et al. 2010; Rigato et al. 2011; Swinnen et al. 2013). Several signaling pathways were recently proposed to be involved in microglia recruitment to the embryonic brain *in vivo*, including components such as colony stimulating factor-1 receptor (CSF1R), matrix metalloproteinases (MMPs), vascular endothelial growth factor receptor (VEGFR), Fractalkine receptor (CX3CR1) and stromal cell-derived factor 1 (SDF-1)/CXCR4 (Arno et al. 2014; Ueno and Yamashita 2014). Cortical colonization depends mainly on microglial invasion and migration since only a minority of these cells proliferates within the parenchyma during this developmental period (Swinnen et al. 2013). Despite the fact that parenchymal migration of microglia is essential to brain colonization, the mechanisms allowing microglial dispersion have never been investigated *in vivo* (Eyo and Dailey 2013; Ueno and Yamashita 2014).

Cell migration relies on interactions with the extracellular matrix (ECM). Cell-ECM adherence is regulated through integrins, which are transmembrane heterodimeric cell adhesion receptors composed of a non-covalently linked α and β subunit. Upon activation, the β subunit physically links the ECM with the cytoskeleton and enables the cell to transduce forces necessary for soma displacement (Vicente-Manzanares and Horwitz 2011). Twenty four different integrin heterodimers

exist in vertebrates with varying ligand binding properties and cell and tissue distributions. They translate ligand binding signals to a broad array of cell responses, such as cytokine production, proliferation, differentiation and migration (Hynes 2002). Our research group previously showed that microglial migration speed changes during cortex colonization in the mouse embryo (Swinnen et al. 2013) which suggests the interaction of microglia with their local environment changes during the course of early development. Several *in vitro* findings point to a possible functional role of microglial interactions with fibronectin (an ECM protein) in migration during embryonic development. Fibronectin, a heterodimeric glycoprotein abundant in most tissues, is an important component of basement membranes. It is expressed in the developing mouse CNS (Lau et al. 2013; Ruoslahti 1996; Sheppard et al. 1991) and is essential for normal embryonic development (Romberger 1997) where it regulates cell differentiation and migration in general (Romberger 1997; Tanzer 2006). Microglia *in vitro* express the corresponding major fibronectin receptor, α5β1 integrin (Milner 2009; Milner and Campbell 2003) and it has been shown *in vitro* that these cells can migrate along fibronectin matrix (Milner and Campbell 2003; Nasu-Tada et al. 2005). Moreover, they can interact with blood vessels that are known to express fibronectin during development (De Gasperi et al. 2012; Grossmann et al. 2002; Milner and Campbell 2002b; Pont-Lezica et al. 2011; Sheppard et al. 1991; Stewart and Pearlman 1987; Tanzer 2006).

Here, we explore the role of microglia-fibronectin interactions, mediated through α5β1 integrin, when the developing embryonic neocortex is colonized by microglia. We use e*x vivo* acute brain slice preparations in order to maintain the physiologic 3D brain environment, which is essential for studying normal migration behavior (Doyle and Yamada 2016; Kasahara et al. 2016; Petersen and Dailey 2004). We first extensively characterize microglial migration behavior at E13.5, E15.5 and E17.5 using 2-photon time-lapse microscopy. We then analyze the presence of fibronectin in the developing cortex using immunofluorescence and western blotting and determine the expression level of α5β1 integrin receptor using flow cytometry on acutely isolated embryonic microglia. Finally,

we assess the functional importance of fibronectin-α5β1 interactions during microglia contact with blood vessels and during parenchymal migration.

MATERIALS AND METHODS

Animals

Wild type *mus musculus* C57BL/6 JOlaHsD females (Harlan, The Netherlands) were mated overnight with CX3CR1$^{eGFP/eGFP}$ knock-in males, obtained from the European Mouse Mutant Archive (EMMA) with the approval of Jung et al. (Jung et al. 2000). The next morning, females were checked for the presence of a copulation plug and designated E0.5. Pregnant mothers were sacrificed at E13.5, E15.5, E17.5 by cervical dislocation. Resulting CX3CR1$^{+/eGFP}$ embryos harbor green fluorescent microglia, monocytes and subsets of natural killer cells and dendritic cells, without the disadvantages of a full CX3CR1 gene deletion (Jung et al. 2000). All experiments were conducted in accordance with the European Community guiding principles on the care and use of animals and with the approval of the Ethical Committee on Animal Research of Hasselt University. Mice were maintained in the animal facility of Hasselt University in accordance with the guidelines of the Belgian Law and the European Council Directive.

Markers

The following primary antibodies were used: anti-fibronectin (1:100 for immunohistofluorescence, 1:1000 for western blotting, #Ab2413, Abcam), anti-β-actin antibody (1:10.000, #Sc47778, Santa Cruz), , anti-α5-Phycoerythrin (clone 5H10-27 (MFR5), 1.5µg/ml, #557447, BD Biosciences). Isolectin GS-IB$_4$ from *Griffonia simplicifolia* conjugated to Alexa568 (5µg/ml for time-lapse imaging, 10µg/ml for immunohistofluorescence, #I21412, Life Technologies) was used to mark blood vessels. For time-lapse blocking experiments, anti-α5β1 (clone BMC5, 10µl/ml, #NBP2-29788, Novus) or isotype control (clone RTK4174, 10µl/ml, #400710, Biolegend) were used. The following secondary antibodies were used for immunohistofluorescence: anti-rabbit-Alexa555 (1:500, #A31572, Life Technologies), anti-rabbit-Alexa647 (1:500, #A21245, Life Technologies); and for western blotting: anti-rabbit and anti-mouse-HRP (1:2000, #P0217 and 1:5000, #P0447, DAKO).

To label fibronectin, we used a polyclonal anti-fibronectin antibody (Li et al. 2016). Fibronectins are disulphide linked heterodimeric molecules of 235–270 kDa. Fibronectin molecular isoforms arise via alternative splicing of a single gene. Specificity was determined by the manufacturer by western blotting on different mouse tissue lysates and a single band was obtained around 250 kDa as predicted for the molecular weight of a single fibronectin subunit (Tanzer 2006). In time-lapse experiments related to microglia-blood vessel contact assessments, isolectin GS-IB_4-Alexa568 was added to the migration medium to visualize blood vessels (Graupera et al. 2008). It is widely used to label blood vessels and microglial cells in slice cultures and does not activate microglial cells (Grinberg et al. 2011). To label α5β1 integrin on microglial cells dissociated from cortex homogenates for flow cytometry, we used a monoclonal anti-α5-Phycoerythrin conjugated antibody (Cukierman et al. 2001). Because the α5 integrin subunit (alternatively named CD49e and VLA-5) exclusively associates with the β1 subunit, we consider its presence to be in heterodimeric form with β1 (Milner and Campbell 2002c).

Time-lapse imaging

E13.5, E15.5 and E17.5 embryonic brains were isolated and sliced as described before (Swinnen et al. 2013). Slices were transferred to MilliCell organotypic inserts (Merck Millipore) in a 24-well plate designed for confocal microscopy (IBIDI) and maintained in semidry conditions as described before (Swinnen et al. 2013). Slicing quality was verified using the dissection microscope and slices that showed aberrant morphology (ruptures, insufficient flatness) were excluded from time-lapse measurements. In blocking experiments, migration medium was supplemented with either a function blocking antibody specifically targeting the α5ß1 integrin dimer (Legate et al. 2011) or with isotype control. Specificity of the α5ß1 antibody was verified by the manufacturer by the antibody's ability to immunoprecipitate α5ß1 heterodimers from (125)-I-surface labelled cells, by reciprocal depletion of α5ß1 antigen from cell lysate with antiserum against the cytoplasmatic domain of the α5 subunit, and by immunoprecipitation of α5ß1 integrin from cells known to express this integrin.

Image acquisition started after 1 h of tissue equilibration at 35°C with 5% CO2 and within 3.5 h after decapitation. During measurements humidified air with 5% CO_2 was continuously applied to the slice, kept at 35°C. Per experiment (1 mother animal), six slices were imaged sequentially and this was repeated every 10 min during 6 h using the '*multitime macro*' in the Zeiss LSM510 software (version 4.2 SP1, Zeiss) on an inverted Zeiss Axiovert 200M microscope with a Zeiss LSM 510 Meta confocal laser scanning system and a 20x EC plan-Neofluar objective (NA of 0.5 and 2 mm working distance). A Mai Tai DeepSee Ti:Saphire laser (Spectra-Physics) with a central wavelength tuned at 900 nm was used to visualize eGFP positive microglial cells and isolectin GS-IB_4-A568 labeled blood vessels. Z-stacks spanning 30 µm, with serial optical sections (voxel size 0.88 x 0.88 x 3.3 µm) were recorded starting from a minimal depth of 50 µm beneath the surface of the slice to avoid cells activated by slicing (Eyo et al. 2014; Schiefer et al. 1999).

Migration tracking and analysis

Image processing and migration tracking were performed using open source Fiji software (ImageJ 2.0.0-rc-643/1.50i). Time series were first corrected for 3D drift using the 3D drift correction plugin and microglial migration was manually tracked in 4D using the MTrackJ plugin designed by Erik Meijering (Meijering et al. 2012). Only cells remaining in the field of view for at least 100 min were included in the analysis. Per experiment, at least one control and/or isotype condition were performed.

Average migration speed (µm/h) was calculated as the total length of the travelled path divided by the duration of the track. The immobile fraction was calculated as the percentage of total microglia that did not migrate further than 45 µm over the total imaging time span. This threshold corresponds to 3 times the average cell diameter and was applied because of small errors due to residual tissue drift after 3D drift correction and manual tracking. Relative idling time was calculated using a custom made Excel macro developed by Gorelik et al (Gorelik and Gautreau 2015) and is defined as the percentage of time the cell spent on pausing, further designated as idling, with regard to the total duration of the track. The threshold for idling was set at roughly half a cell diameter (8 µm) per 10

minutes and was verified by inspecting subsequent displacements of non-migratory cells in MTrackJ. Instantaneous speeds of the active migration events ($v_{inst.\ act.}$ = µm/min), i.e. events above the idling threshold of 0.8 µm/min, were calculated as the distance travelled between each time frame, divided by the frame interval (10 min). Migration parameters are grouped under treatment and age. At least 8 slices from embryos of 5 different mothers were quantified.

Fixed tissue preparation and immunohistofluorescence

Pregnant mice were sacrificed and embryonic tissue was processed as described before (Swinnen et al. 2013). 10-20 µm coronal sections were cut on a Leica CM3050S cryostat, mounted on Superfrost Plus slides (ThemoFisher) and stored at −20°C until staining. For fibronectin stainings, sections were washed and blocked during 1 h with PBS-20% NXS (Normal Goat or Donkey Serum, Chemicon). All steps occurred at room temperature (RT) unless stated otherwise. Primary antibody was diluted in PBS-1% NXS and incubated overnight at 4°C. For fibronectin-isolectin GS-IB_4 double labelling, the isolectin was incubated at 10µg/ml together with the primary antibody overnight at RT. Sections were washed 3 x 10 min in PBS and incubated 1 h with the secondary antibody diluted in PBS-1% NXS. Sections were washed 3 x 5 min in PBS, submerged in distilled water and mounted using vectashield including 4,6-diamidino-2-phenylindole (DAPI) (Vector, Burlingame). For negative controls, primary antibodies were omitted. Secondary antibodies were centrifuged 5 min at 5000 revolutions per minute prior to use.

Microscopy and mean grey value assessment

Images of fibronectin immunostainings were acquired using a Digital sight DS-2MBWc fluorescence camera adapted on a Nikon Eclipse 80i microscope. Fibronectin presence was quantified in the embryonic cerebral cortex area located dorsally to the lateral ganglionic eminences (LGE) and medial ganglionic eminences as previously described (Swinnen et al. 2013). Background signal was determined using the line plot profile tool in Fiji for each image separately. Signal below 2.5 times the background was removed. In each slice a region of interest (ROI; white dotted lines Fig. 3A) was

determined including the entire cortex but excluding the meninges. The mean grey value, defined as the average grey value of all pixels inside the ROI, was assessed using the '*Measure*' function in Fiji. These measurements resulted in a mean grey value per pixel (0.16 µm²) automatically corrected for the surface of the ROI and therefore also for the size of the growing cortex. Slices were from 3 different embryos of at least 2 different mothers.

Images of fibronectin-isolectin GS-IB_4-A568 double immunostainings (20 µm tissue sections) were acquired using an inverted Zeiss Axiovert 200M microscope with a Zeiss LSM 510 Meta confocal laser scanning system. An Arg-ion laser at 488 nm, a HeNe laser at 543 and 633 nm and a Mai Tai DeepSee Ti:Saphire laser (Spectra-Physics) tuned at 710 nm were used for excitation of eGFP, Alexa568, Alexa647 and DAPI, respectively. Overview pictures (voxel size 0.44 x 0.44 x 1 µm; 10-15 µm Z-stacks) were acquired using a 40x LD C-Apochomat/1.1 W Korr UV-Vis-IR objective (NA=1.1) with the Zeiss Laser scanning microscope LSM510 software. A 4x confocal zoom was applied to cells of interest (voxel size 0.11 x 0.11 x 2 µm).

Western blotting

Embryonic brains were isolated as described before (Swinnen et al. 2013), the meninges were removed, cortices were excised and stored at -80°C. Cortices were lysed in cold RIPA buffer (50mM Tris pH 7.4; 150mM NaCl; 1mM EDTA; 1% NP-40; 0.25% Na-deoxycholate; protease inhibitor (#11873580000, Roche)). Protein concentrations of individual cortices were determined by the BCA protein assay kit (#23225, Thermo Fisher). Samples containing equal amount of proteins (10 µg) were separated on a 12% SDSPAGE gel, transferred to a polyvinylidene fluoride (PVDF) membrane and blocked for 1 h with Tris buffered saline-0.1% Tween 20 (TBS-T) containing 5% milk powder (Marvel) followed by incubation overnight at 4°C in the presence of anti-fibronectin antibody. Mouse anti-β-actin antibody was subsequently incubated for 2 h followed by horseradish peroxidase-conjugated secondary antibodies incubation for 1 h. All antibodies were diluted in blocking buffer and incubations were at RT unless stated otherwise. Enhanced chemiluminescence using the Pierce ECL

Plus Western Blotting Substrate (#32132, Thermo Scientific) was used before imaging with the ImageQuant LAS4000 mini (GE Healthcare Life Sciences). Quantification was performed using ImageQuantTL.

Microglia isolation and flow cytometry

Cortical microglia from CX3CR1$^{+/eGFP}$ E13.5, E15.5 and E17.5 brains were isolated as described before (Smolders et al. 2015) with modifications. The tissue was mechanically homogenized in neurobasal medium (Gibco, Thermo Fisher Scientific) supplemented with 2mM L-glutamine, N2 supplement, B27 supplement and 1% penicillin/streptomycin (all from Thermo Fisher Scientific). The homogenate was centrifugated 5 min at 700 g at 4°C, the pellet was resuspended in cold PBS and stained with Fixable Viability stain 620 (FVS620) (BD Biosciences) during 10 min at RT. Cell suspensions were fixed in 4% PFA during 10 min, washed and dissolved in PBS. Cells were incubated for 15 min on RT with an α5-Phycoerythrin conjugated antibody in PBS. After washes, cells were acquired in a FACS Fortessa (BD Biosciences) and analyzed with FACS Diva 8.0.1 software (BD Biosciences). Within the living cell population (FVS620 low) the eGFP positive microglia (110-4799 cells per tube) were gated. Within the microglial population, the percentage of α5 positive microglia and its median fluorescence intensity (MFI) were analyzed. Because α5 measurements were part of a panel not further described here, Fluorescence-minus-one (FMO) controls (for justification see (Maecker and Trotter 2006)) were used to gate the positive cell population. At E13.5, embryos were pooled per 2 or 3 (N=8). At E15.5 (N=16) and E17.5 (N=20), embryos were analyzed separately. Data were obtained from 3 different mothers (M=3).

Microglia-blood vessel contact analysis

To quantify microglia-blood vessel interactions, we added isolectin GS-IB$_4$-A568 (see section 'Time-lapse imaging') in the imaging medium 1 h prior to imaging onset to visualize blood vessels. Quantification occurred on the 30 µm Z-stacks acquired from 3 h after onset of imaging, in order for the GS-IB4 labeling to sufficiently penetrate the tissue, until 6 h. Only cells located in the parenchyma

and that were visible during at least 9 subsequent time points were included in the analysis. For each cell throughout the Z-stack at each time point, the type of contact was noted as full soma, touching with a process or no contact (free). Microglia that made contact with a blood vessel (soma or process) during 1 or more frames, were considered to be in contact with blood vessels for the analysis in Fig. 4C and a percentage was calculated per slice. The percentage of time each cell spent on a particular contact (Fig. 4D) was calculated and data from cells were pooled per treatment and age. At least 7 different embryonic brain slices (N=7) of 3 different mothers (M=3) were quantified per treatment. All blood vessel contact analyses were performed blinded.

Statistical analysis

The number of analyzed cells or steps is indicated as "n", the number of embryos or slices as "N" and the number of mothers as "M". The #cells/#embryos or slices/#mothers is thus designated in the text as n/N/M unless stated otherwise. The reader is referred to the figure legends for details about the sample size used for statistical analysis. Data are described in the text as "median [interquartile range (IQR)]" according to standards for describing nonparametric data (Madadizadeh et al. 2015). Statistical analyses and graphs were produced using SAS JMP® Pro 12.1.0. Data are represented as box plots with whiskers to 1.5x the IQR (Tukey representation). Data distributions were assessed for normality (Shapiro-Wilk) and equality of variance (Brown-Forsythe). In case these assumptions were met for all groups, a Student *t*-test in case of 2 groups or ANOVA was performed in case of three groups followed by Tukey HSD post-hoc, correcting for multiple comparisons. In Fig. 3D and 3H, data were transformed on a log10 scale to meet the equality of variance assumption, though the original scales were used for data presentation for ease of interpretation. When data distribution of least one group was non-gaussian, nonparametric tests such as Mann-Whitney in case of two groups or Kruskal-Wallis with Dunn's multiple comparison post-hoc in case of three groups were performed. *P*-values smaller than 0.05 were considered significant with * $P<0.05$, ** $P<0.01$ and *** $P<0.001$.

RESULTS

Microglial migration speed decreases with development

Microglial colonization of the embryonic mouse brain cortex occurs in three phases based on microglial density: an initial phase of fast increasing cell density from E10.5 until E14.5, followed by a plateau phase between E14.5 and E15.5, and a third invasion phase after E15.5 (Swinnen et al. 2013). During mammalian development these cells are already highly mobile, with the capacity to phagocytose dying cells and scan the microenvironment as observed in the adult brain (Eyo and Dailey 2013; Nimmerjahn et al. 2005; Swinnen et al. 2013; Zhang et al. 2016). Two-photon time-lapse microscopy was used in this study to investigate developmental changes in microglial migration within the time frame of ongoing neuronal migration (Greig et al. 2013; Swinnen et al. 2013). To this end, acute brain slices obtained from E13.5, E15.5 and E17.5 CX3CR1$^{+/eGFP}$ embryos were used, representing the 3 aforementioned phases in microglial development. Migration was analyzed starting from E13.5, because on E12.5 very few cells reside yet in the cortical parenchyma and mobility is low (Swinnen et al. 2013). We focused our analysis on the cerebral cortex area located dorsally to the lateral ganglionic eminences (LGE) and medial ganglionic eminences (MGE) (see also Fig. 3A a1, b1 and c1) (Swinnen et al. 2013). Representative Z-projections of time-lapse experiments with overlaid migration tracks are shown for each age in Figure 1A.

The cell average migration speed within one brain slice was highly variable (Fig. 1B). The median average speed at E13.5 (33.4 µm/h [IQR: 22.5-44.4]) did not differ significantly from the speed at E15.5 (33.63 µm/h [IQR: 21.2-47.4]) (Fig. 1B and C). At E17.5 average migration speed significantly decreased (24.2 µm/h [IQR: 15.7-34.3]) compared to E13.5 and E15.5 (Fig.1B and C). The decrease in speed suggests that with development, microglia start to acquire their final locations. To evaluate this presumption, we analyzed the percentage of immobile cells per slice from E13.5 to E17.5 and found that the immobile fraction rose significantly from 0.0% [IQR: 0.0-2.1] at E13.5 to 9.1% [IQR: 3.1-15.1] at E17.5 (Fig.1D). To rule out that the decrease in migration speed was solely due to an

increase in immobile fraction, we reassessed the average migration speed of the mobile fraction. We also found a significant decrease in speed with development (E13.5 vs. E17.5 or E15.5: $P<0.001$, Kruskal-Wallis with Dunn's post test) (data not shown).

The parallel decrease in migration speed and increase in immobile fraction suggest that microglial migration speed is developmentally regulated during early colonization of the embryonic cortex.

Microglia adopt a saltatory migration pattern over development

In their migration process microglia first scan their environment, send out one or multiple processes, and displace their soma in the direction of one of the protrusions while retracting the others. Subsequently the cell idles, i.e. the migration of the cell body pauses, explores the environment again and the cycle is repeated (Fig. 2A). This locomotion pattern can be described as saltatory and was observed at each age tested. To visualize this saltatory behavior, the speed between two subsequent time points, defined as instantaneous speed, was plotted in function of time for three microglial cells that are representative for cells with high, intermediate and low average speeds (Fig. 2B). To better characterize the saltatory behavior over development and to find the underlying mechanism of changes in average speed, the median relative idling time and the median instantaneous speed of the migration events above the idling threshold were determined (Gorelik and Gautreau 2015). For example, average speed can be decreased because the cells spend more time idling, and/or because when migrating, distances between subsequent time points become shorter. The relative idling time was calculated as the percentage of the time the cell spends on idling with regard to the total track duration (Gorelik and Gautreau 2015) and was significantly increased over development (E13.5: 77.0% [IQR: 64.3-88.6], E15.5: 74.3% [IQR: 63.2-86.1], E17.5: 82.8% [IQR: 72.8-91.7]) (Fig. 2C). Instantaneous speed (µm/min) was calculated as the travelled distance between subsequent time points, divided by the frame interval and was found to be significantly decreased only between E15.5 (1.4 µm/min [IQR: 1.1-2.0]) and E17.5 (1.3 µm/min [1.0-1.8]) (Fig. 2D and E).

Our results thus show that microglia during early colonization of the embryonic cortex migrate with jumps and that the developmental decrease in microglial average migration speed is due to the cells spending more time pausing and additionally migrating in smaller steps.

Cortical fibronectin presence decreases over development

Developmental changes in microglial migration might result from changes in the microenvironment. ECM proteins, such as fibronectin, are developmentally regulated (Sheppard et al. 1991). Nevertheless, the deposition pattern of fibronectin in the embryonic mouse brain remains controversial (De Gasperi et al. 2012; Sheppard et al. 1991; Stewart and Pearlman 1987). To bring clarity on this pattern at the ages relevant for this study, fibronectin's deposition pattern in the embryonic cortex during the microglial colonization phase from E13.5 to E17.5 was analyzed using immunostaining (Fig. 3A) and cortical mean grey value quantification (Fig. 3B). Fibronectin was localized throughout the entire cortex at E13.5 as thick aggregates (Fig. 3A, a1-a4). At E15.5 (Fig. 3A, b1-b4) and E17.5 (Fig. 3A, c1-c4), fibronectin staining was less dense when compared to staining at E13.5. Mean grey value assessment (gray value scale 0-255; immunostaining intensity) indicated that fibronectin deposition decreased (Fig. 3B) during the microglial colonization phase of the embryonic cortex. The median cortical fibronectin grey values were 13.8 [IQR: 11.7-7.2] at E13.5, 8.5 [IQR: 6.2-11.5] at E15.5 and 2.9 [IQR: 1.4-5.4] on E17.5, which all significantly differ from each other (Fig. 3B). To confirm the mean grey value measurements, the fibronectin protein content was determined on isolated embryonic cortices using western blotting (Fig. 3C). Quantification of fibronectin relative to β-actin showed that the cortical fibronectin contents at E13.5 (51.6 [IQR:33.1-77.3]) and at E15.5 (32 [IQR:22.9-37.9]) were significantly higher than at E17.5 (7.6 [IQR:4.3-17]) (Fig. 3D).

Though fibronectin was diffusely localized in the parenchyma, developing blood vessels marked by isolectin-GS-IB_4 (Fig. 3E, e4) were highly immunoreactive for fibronectin (Fig. 3E, yellow arrowheads in e1, e3 for zoom-in), as reported extensively in literature (De Gasperi et al. 2012; Milner and Campbell 2002b; Sheppard et al. 1991; Stewart and Pearlman 1987). As previously described

(Grossmann et al. 2002; Kierdorf et al. 2013; Pont-Lezica et al. 2011; Rigato et al. 2011) microglia were often found in close proximity with blood vessels (Fig. 3E).

Thus, cortical fibronectin decreases with development and it is also deposited along blood vessels.

Fibronectin receptor α5β1 is expressed by microglia and is developmentally downregulated

Microglia-ECM contacts are likely to be mediated by fibronectin-integrin interactions. *In vitro* adhesion of microglia to a fibronectin coated surface is regulated through fibronectin receptors, such as α5β1 integrin (Milner 2009; Milner and Campbell 2002a; Milner and Campbell 2003; Welser-Alves et al. 2011). This integrin heterodimer is described as the major fibronectin receptor and is well characterized on the molecular as well as the signaling level (Bachman et al. 2015; Hynes 2002). To determine the expression of α5β1 integrin on embryonic microglia *in vivo*, E13.5, E15.5 and E17.5 cortices were isolated and the fibronectin receptor was immediately analyzed after isolation using flow cytometry. Because the α5 integrin subunit exclusively associates with the β1 subunit, a monoclonal antibody raised against α5 was used to identify α5β1 expression on microglial cells (Milner and Campbell 2002c). Microglial cells were gated based on eGFP expression, after exclusion of dead cells (Fig. 3F). At E13.5, 99.8% [IQR: 98.8-100.0] of the microglial population expressed the α5 subunit (Fig. 3G). This percentage did not change at E15.5 (99.9% [IQR: 99.5-100.0]), but it was significantly different at E17.5 (98.9% [IQR: 97.6-99.4]) compared to E15.5 (Fig. 3G). The median fluorescence intensity (MFI), an indicator of the expression level per cell, of the α5 positive microglia significantly decreased from E13.5 (12356 MFI [IQR: 11678-14330]) to E15.5 (9558 MFI [IQR: 8825-10207]) and to E17.5 (4479 MFI [IQR: 4202-4796]) (Fig. 3H).

In conclusion nearly all embryonic microglia expressed the α5β1 integrin receptor but the expression level decreased in the course of development.

α5β1 integrin is dispensable for microglia contact with blood vessels

Microglia are often observed in contact with blood vessels in the developing and adult CNS and in physiologic as well as in pathologic conditions (Arnold and Betsholtz 2013; Grossmann et al. 2002; Pont-Lezica et al. 2011). However, the mechanical basis for this contact is unknown (Arnold and Betsholtz 2013; Dudvarski Stankovic et al. 2016; Pont-Lezica et al. 2011). Based on our previous findings, the α5β1 integrin was suspected to mediate microglia attachment to blood vessels. Since microglia were reported to migrate along blood vessels after injury in rat postnatal slice preparations (Grossmann et al. 2002) and they made transient contacts with blood vessels in the developing zebrafish from 6 to 10 days post fertilization (dpf) (Svahn et al. 2013), it was first determined whether α5β1 integrin could be important in the capability of microglia to migrate along blood vessels. Time-lapse imaging showed that microglia can use blood vessels as substrates to migrate in the cortex of the mouse embryo (Fig. 4A upper panel, Suppl. Movie 1). However, α5β1 blockage using a blocking antibody specifically targeting the α5β1 integrin dimer did not impair this capability of microglia to migrate along the surface of blood vessels (Fig. 4A lower panel, Suppl. Movie 2). To confirm this observation, the percentage of microglia contacting a blood vessel was determined in the time-lapse sequences starting from 3 h after application of the α5β1 blocking. Two modes of contact were observed: full soma alignment (Fig. 4B left panel) and “touching” contacts between blood vessels and microglial cell processes (Fig. 4B middle panel). Because the process contact mode was less frequently observed, both contact modes were grouped under “microglia-blood vessel contact”. For comparison purposes, a free microglia not contacting a blood vessel is shown in Figure 4B (right panel). At E13.5 and E17.5, 50.0% [IQR: 36.7-81.3] and 100% [IQR: 85.1-100.0] of microglial cells contacted blood vessels in the presence of the isotype and the percentage did not change after α5β1 blockage (E13.5: 50.0% [IQR: 40.0-66.7], E17.5: 86.6% [IQR: 61.1-100.0]) (Fig. 4C). The percentage of microglia contacting blood vessels significantly increased with development (Fig. 4C).

Blocking α5β1 might have subtle effects on microglia behavior, such as dynamic changes in contacts with blood vessels, which cannot be revealed by the analysis described above. Therefore we next investigated the percentage of time that each cell spent on contacting blood vessels - either by full soma contact, process contact or no contact as illustrated in Figure 4B. The percentage of time spent on a particular contact was highly variable (Fig. 4D). At E13.5 in control conditions, the median percentage of time microglia spent on contacting a blood vessel using their soma or using processes was 0.0% [IQR: 0.0-92.1] and 0.0% [IQR: 0.0-5.3], respectively. 84.2% [0.0-100.0] of the time, the cells made no contact. These values did not change after α5β1 blockage (5.3% [0.0-89.9], 0.0% [0.0-5.8] and 84.2% [5.6-100.0], for Soma, Process or no contact, respectively). At E17.5 in control conditions, the median percentage of time microglia spent on contacting a blood vessel using their soma or using processes was 21.1% [IQR: 0.0-80.3] and 21.1% [IQR: 0.0-48.7], respectively. 23.7% [0.0-63.2] of the time, the cells made no contact. These values did not change after α5β1 blockage (20.5% [0.0-59.2], 25.7% [0.0-54.0] and 10.5% [0.0-79.0], for Soma, Process or no contact, respectively).

All together, these results indicate that α5β1 integrin is neither essential for the capability of microglia to migrate along blood vessels nor for microglia-blood vessel contact.

α5β1 integrin blockage has opposite effects on microglia migration during the embryonic cortical development

Based on the parallel decrease in microglial average migration speed, cortical fibronectin deposition and α5β1 integrin expression level on microglia during the developmental period analyzed, it was hypothesized that the functional importance of this receptor during microglial migration would diminish over time. To address this issue, the same migration parameters as analyzed for control migration (Figs. 1 and 2) were assessed, but in the presence of the α5β1 blocking antibody or isotype control in E13.5, E15.5 and E17.5 acute brain slices (Fig. 5, Suppl. Movies 3 to 8). Representative time-lapse Z-projections overlaid with migration tracks are shown in Fig. 5A. There was no effect of isotypes on migration (Fig. 5B; Fig. 6; Fig. 1B).

At E13.5 α5β1 integrin blockage caused a significant reduction (~25%) of the average migration speed (23.5 µm/h [IQR: 15.7-37.8]) when compared to isotype control (31.5 µm/h [IQR: 19.6-44.0]) (Figs. 5B and D). Conversely, α5β1 integrin blockage at E15.5 and E17.5 significantly increased the migration speed to 41.3 µm/h [IQR: 27.8-56.7] (~14%) and 31.6 µm/h [IQR: 19.7-50.9] (~17%) compared to isotype (E15.5: 36.2 µm/h [IQR: 23.7-49.3], E17.5: 27.0 µm/h [IQR: 17.7-37.2]) (Figs. 5B, 5D). The effect of the antibody was indeed significantly different across ages (dotted lines with asterisks, Fig. 5B). Upon α5β1 blockage, the immobile fraction was 0.0% [IQR: 0.0-9.1] at E13.5, 0.0% [IQR: 0.0-8.3] at E15.5 and 3.1% [IQR: 0.0-8.0] at E17.5, which were not significantly different from isotype (0.0% [IQR: 0.0-13.2] at E13.5; 5.0% [IQR 0.0-7.7] at E15.5 and 5.0% [IQR: 0.0-10.9] at E17.5) (Fig. 5C). The effect of the antibody did not differ across ages. After exclusion of the immobile fraction in the average speed analysis, we found the same significant differences between isotype and α5β1 blockage (E13.5: P=0.016, E15.5: P=0.013, E17.5: P<0.001, Kruskal-Wallis with Dunn's post test) (data not shown). This confirms that α5β1 blockage does not affect the immobile microglial population.

These results indicate that α5β1 integrin blockage affects the microglial average migration speed in opposite ways depending on the embryonic age, without affecting the proportion of immobile microglia.

To determine whether the change in average speed was due to the cells spending more or less time idling and/or to a change in instantaneous speed, we determined the median relative idling time and the median instantaneous speed of the events above the idling threshold (Fig. 6). After α5β1 blockage, the median relative idling time was 84.6% [IQR: 72.1-91.7] at E13.5, 67.4% [IQR: 51.9-78.9] at E15.5 and 77.0% [IQR: 60.1-86.2] at E17.5 (Fig. 6A). They were all significantly different compared to isotype (76.9% [IQR: 66.6-88.3] at E13.5, 71.8% [IQR: 60.0-83.8] at E15.5 and 80.0% [IQR: 70.6-88.9] at E17.5). After α5β1 blockage the instantaneous velocities of migration events were 1.3 µm/min [IQR: 1.0-1.9] at E13.5, 1.4 µm/min [IQR: 1.1-2.0] at E15.5 and 1.4 µm/min [IQR: 1.1-2.1] at

E17.5 (Fig. 6B and C). Only at E17.5, after blockage microglia migrated with a significantly higher instantaneous speed compared to isotype control (1.4 µm/min [IQR: 1.0-2.0] at E13.5, 1.5 µm/min [IQR: 1.1-2.0] at E15.5, 1.4 µm/min [IQR: 1.0-1.8] at E17.5) (Fig. 6B and C). Additionally, after α5β1 blockage at all ages, microglia still migrated saltatory (see all Supplementary Movies).

In conclusion, α5β1 blockage mainly affects the time the cells spend idling without affecting the saltatory migration pattern.

DISCUSSION

In this study, we show that during early colonization of the embryonic cortex microglia migrate in a saltatory fashion and that their average migration speed is developmentally regulated. We demonstrate that the adhesion molecules fibronectin and its receptor the α5β1 integrin play an important role in regulating embryonic microglial migration. The presence of cortical fibronectin and the expression of α5β1 integrin on microglia decreased throughout development, but as a paradox we found that α5β1 integrin has opposite functions in microglial migration depending on the embryonic age. Blockage of the α5β1 integrin decreased migration speed at E13.5 while it led to an increased migration speed at E15.5 and E17.5, without affecting the size of the immobile fraction.

Microglia exhibit a saltatory migration behavior while speed decreases during embryonic corticogenesis

The behavior of microglial cells invading the embryonic cortex from E13.5 to E17.5 is characterized by a saltatory migration pattern. This pattern consists of pausing phases during which the microglial cell explores its surroundings interspersed with active phases of migration in the direction of a selected protrusion. This saltatory migration pattern of microglia in the mouse embryonic brain, which is maintained during the developmental period studied here, is similar to the migration behavior of microglia described *in vivo* in the developing zebrafish larvae (Sieger et al. 2012), suggesting that this particular behavior of microglia during brain development is evolutionary conserved over species.

We observed a decrease in the microglial average migration speed over embryonic development and this resulted from both an increased idling time and a lower instantaneous speed. Our observations are similar to what has been observed between postnatal ages P2 and P6 in the mouse hippocampus (Eyo et al. 2016) and between 3.5 and 5 dpf in the zebrafish optic tectum (Svahn et al. 2013). The decrease in average speed at E17.5 coincided with an increase in the immobile fraction of microglial cells and could indicate that some microglial cells acquire their final locations in the cortex between E13.5 and E17.5. However, we cannot exclude that the rise in immobile fraction over early development reflects a long lasting transitory resting state between active migration phases, since

the cortical development proceeds postnatally (Finlay and Darlington 1995; Sauvageot and Stiles 2002). The immobile fraction was insensitive to α5β1 blockage from E13.5 to E17.5. This suggests that α5β1 does not essentially contribute to the integrin-ECM interactions tightly anchoring the cell in place. The decrease in microglial migration speed is likely to result from changes in the local environment. We show that the fibronectin deposition and the expression of fibronectin receptor α5β1 integrin on microglia, decrease from E13.5 to E17.5 in the cortex. Indeed, changes in ECM composition alter microglial adhesion to substrates, which could impact their migration (Milner and Campbell 2002c; Milner et al. 2007). Accordingly microglial migration speed was decreased in the newborn rabbit brain as a consequence of *in utero* inflammation and it was suspected to result from changes in adhesion molecule expression after inflammation (Zhang et al. 2016).

Developmental decrease in fibronectin and microglial fibronectin receptor α5β1 integrin expression in the embryonic cortex

All three parameters, microglial average migration speed, the cortical fibronectin deposition and microglial α5β1 integrin expression levels decreased from E13.5 to E17.5. This concurrent decrease indicates that the interaction between fibronectin and α5β1 integrin might regulate microglia migration speed supporting the hypothesis that the ECM plays an important role in migration during early colonization of the cortex by these immune cells. Throughout development, fibronectin is highly expressed by blood vessels and along radial glial processes (De Gasperi et al. 2012; Milner and Campbell 2002b; Sheppard et al. 1991; Stewart and Pearlman 1987), which makes these structures ideal scaffolds to guide microglial migration. Accordingly, changes in microglial migration speed observed in the presence of the α5β1 integrin blocking antibody may result from an alteration of interactions between microglia, blood vessels and/or radial glial fibers.

No role for α5β1 integrin in mediating microglial contact with blood vessels

Contact between microglia and blood vessels during development has been reported in zebrafish, quails, mice, rats as well as humans (Pont-Lezica et al. 2011). Although α5β1 integrin is implicated in the adhesion of CNS endothelial cells to fibronectin (Milner and Campbell 2002b), we did not find any evidence for a role of this receptor in the dynamic interaction between microglia and blood vessels during the developmental period investigated here. Neither the capability of microglia to use blood vessels as guiding substrates for migration, nor the fraction of these cells contacting blood vessels, nor the time spent on soma or process contact was altered in the presence of the blocking antibody. Other ECM proteins, such as laminin or Intercellular Adhesion Molecule (ICAM)-1 or 2, expressed along developing blood vessels might mediate contact (Dalmau et al. 1997; Rezaie et al. 1997) as microglia *in vitro* do express the receptors for these ligands (Dalmau et al. 1997; Milner and Campbell 2003). Additionally, integrins other than α5β1 might be involved in adhesion to fibronectin expressed by blood vessels (Milner and Campbell 2003; Welser-Alves et al. 2011). Lack of effect of the blocking antibody on microglia interaction with blood vessels does not preclude disturbances of microglial interactions with other cell types, such as radial glia which produce and align fibronectin along their processes (Sheppard et al. 1995; Sheppard et al. 1991; Stettler and Galileo 2004). Dense packing of these radial glial fibers may however hamper reliable quantification of interactions with microglia in the cortex.

Age-specific role of α5β1 integrin in microglial migration

Although almost all microglia from E13.5 to E17.5 expressed α5β1 integrin, its expression level decreased over development. This might indicate that embryonic microglia are capable to interpret changes in fibronectin deposition. This idea is supported by *in vitro* work showing that after cultivation on fibronectin primary microglia upregulate α5β1 integrin (Milner and Campbell 2003). Based on the developmental decrease in both adhesion molecules, we expected that blocking α5β1 would largely decrease migration speed at E13.5 while it would affect migration less at E17.5.

Surprisingly our experiments indicate that this is not the case. After α5β1 blockage, migration speed indeed decreased at E13.5, but it increased at E17.5.

Changes in microglial migration speed observed in the presence of the blocking antibody are apparently modest (14-25% changes), but they are in the range of those observed on neurons migration speed after blocking glycine receptors (Avila et al. 2013) or on microglia migration after blocking the CC chemokine receptor 5 (Carbonell et al. 2005). It is likely that α5β1 integrin is not the sole integrin dimer to play a role in microglial migration (Milner and Campbell 2002b). The long term consequences of defective integrin dependent microglial migration on brain development and neuronal network functionality remain unknown and require further attention. This might be a challenging task regarding the fact that genetically engineered integrin knock-outs can suffer from functional compensation of other integrins (Schmid and Anton 2003; Zent 2010).

As observed here at E13.5, a decrease in migration after either α5β1 or general β1 integrin blockage was also reported *in vitro* in microglial chemotaxis and wound healing assays (Kim et al. 2014; Nasu-Tada et al. 2005; Yao et al. 2013). Integrin blockage has led to various outcomes on migration depending on the cell type, the integrin heterodimer and the environmental dimensions. For example α5β1 depletion inhibited neuronal migration during mouse embryonic corticogenesis *in vivo* (Marchetti et al. 2010). On the contrary, integrin blocking antibodies increased migration in platelets (Moroi et al. 2000), neutrophiles (Toyjanova et al. 2015), cancer cells (3D matrix) (Costa et al. 2013) and trophoblast cells (Zhao et al. 2012) *in vitro*, as observed in our experiments at E17.5.

The observed opposite functions of α5β1 integrin during cortical development might be explained by a maturation of the adhesion involving α5β1. Generally, cell migration involves unstable nascent adhesion (physical interaction between the ECM, the integrin and the cytoskeleton) formation which undergoes rapid turnover. When a protrusion rests, the nascent adhesion can “mature” into a highly stable focal adhesion. This means the adhesion grows in size and stability by attraction and posttranslational modifications of intracellular adaptor proteins that constitute the link between the

integrin and the cytoskeleton. When the cell migrates further, the ECM-cytoskeleton link is disrupted (Lock et al. 2008; Vicente-Manzanares and Horwitz 2011). The stability of the adhesion is important for overall cell migration speed and can be regulated at the level of the ECM, the integrin and the adaptor proteins (Doyle and Yamada 2016; Fraley et al. 2010; Lock et al. 2008; Vicente-Manzanares and Horwitz 2011). Interestingly, adhesion strength has a biphasic effect on migration speed: the speed increases between low and intermediate adhesion strength and slows down between intermediate and high adhesion strength (Barnhart et al. 2011; Vicente-Manzanares and Horwitz 2011). We therefore speculate that at E13.5 α5β1 is involved in unstable adhesions which favor migration while from E15.5 onwards, the integrin is linked to more stable, mature adhesions that cause tighter anchoring of the cell body. When the ability to form these unstable adhesions is impaired upon blockage at E13.5, the cell will not find an anchor point to transduce force in order to migrate. At E17.5 α5β1 linked adhesions would be more stable, causing a decrease in migration speed. When the integrin-matrix link is disrupted by the blocking antibody, microglia could be released and could be free to migrate faster using other integrins. Plausible candidates for mediating migration could be α4β1, α6β1, αvβ1, αvβ3, αvβ8, αLβ2 or αMβ2, since microglia express these integrins at least *in vitro* (Milner 2009; Milner and Campbell 2002a; Milner and Campbell 2003). Alternatively, the fibronectin concentration could determine whether α5β1 integrin promotes or inhibits migration, as observed for cultured glioblastoma cells (Blandin et al. 2016).

Migrating neurons, radial glia and blood vessels in the developing brain are known to express the α5β1 integrin (Marchetti et al. 2010; Milner and Campbell 2002b; Yoshida et al. 2003) which could indirectly interfere with the alteration of microglia migration we observed in the presence of the blocking antibody. This is unlikely to be the case at the blood vessel level since we did not observed any difference in microglia-blood vessels interactions in the presence of the blocking antibody. Knock-down of this integrin in neural precursors resulted in a decreased radial migration and affected their morphology and differentiation capacity (Marchetti et al. 2010). To our knowledge it is yet unknown if neuronal migration can affect microglia mobility. So far it has been shown that SDF-1-

expressing basal progenitors in the ventricular/subventricular zone (VZ/SVZ) promotes microglia recruitment into the SVZ (Arno et al. 2014). Nevertheless, we cannot completely exclude that interactions between developing neurons and microglia might be altered after blockage. Finally β1 integrins in radial glia control the morphological differentiation of both glia and neurons (Belvindrah et al. 2007) but the alterations of these processes by impairing β1 integrin expression occur in a time scale that is incompatible with the time scale observed for microglia behavior alteration.

Conclusions

This study is the first to dig deeper into molecular mechanisms of physiologic migration of microglia during development. A limitation of the use of brains slices in this study might be that microglial migration in slice preparations does not reflect the true physiologic behavior during development. Microglia at the slice surface could be activated in terms of phagocytosis and velum-like pseudopod formation as observed in slices of rat facial nucleus following peripheral axotomy (Schiefer et al. 1999). Nevertheless, microglia within the tissue depth did not show such behaviors. This indicates that deep tissue imaging, as performed in our study, is likely to allow analyzing behavior of the microglial population close to physiologic conditions (Eyo and Dailey 2013; Eyo et al. 2016; Schiefer et al. 1999). It is important to note that microglial mobility in the *in vivo* developing zebrafish was also high (Sieger et al. 2012; Svahn et al. 2013). Finally, an *in utero* embryonic brain imaging (Yokota et al. 2007; Yuryev et al. 2015), although challenging, would be required to fully confirm that the intense microglial migration behavior we observed in slices truly reflects the microglial behavior in the developing brain of the intact embryo.

In conclusion, our results strongly indicate that α5β1 integrin regulates the microglial migration process during embryonic microglial colonization of the mouse cortex, without taking part in contact with blood vessels. We report for the first time opposing age-dependent functions of the α5β1 integrin. At E13.5 the α5β1 integrin promotes while at E15.5 and E17.5 it inhibits microglial migration. We hypothesize that during development, the stability of the α5β1-linked adhesion

changes and therefore blockage of the fibronectin receptor leads to different outcomes. What causes microglial migration to decrease and how changes in α5β1 integrin function are molecularly regulated - cell intrinsically and/or environmentally - are questions that require further investigation.

4) Acknowledgements

We sincerely thank Elissia Ventriglia and Rosette Beenaerts for technical assistance with western blotting and tissue isolations. We also thank Dr. Ariel Avila for help with initial set-up of migration experiments, Dr. Rik Paesen for problem shooting with the multiposition macro in the Zeiss software, Jeroen Vrancken for writing Excel macros and Wilfried Lemmers for proofreading the manuscript. Financial support for this research was granted by Impulse financing tUL (transnationale Universiteit Limburg), UHasselt (BOF13N01, BOF16NI04), Research Foundation of Flanders (FWO G0A0513), the Interuniversity Attraction Poles Program – Belgian State – Belgian Science Policy (IAP-P6/31 and P7/10), Agency for Innovation by Science and Technology (IWT O&O JJDDIPS) and Rotary campaign "Hope in Head". We thank Boehringer Ingelheim Fonds and FWO to fund travel for courses and research stays abroad that led to this publication. The authors have no conflict of interest to declare.

5) References

Arno B, Grassivaro F, Rossi C, Bergamaschi A, Castiglioni V, Furlan R, Greter M, Favaro R, Comi G, Becher B and others. 2014. Neural progenitor cells orchestrate microglia migration and positioning into the developing cortex. Nat Commun 5:5611.

Arnold T, Betsholtz C. 2013. The importance of microglia in the development of the vasculature in the central nervous system. Vasc Cell 5:4.

Avila A, Vidal PM, Dear TN, Harvey RJ, Rigo JM, Nguyen L. 2013. Glycine receptor alpha2 subunit activation promotes cortical interneuron migration. Cell Rep 4:738-50.

Bachman H, Nicosia J, Dysart M, Barker TH. 2015. Utilizing Fibronectin Integrin-Binding Specificity to Control Cellular Responses. Adv Wound Care (New Rochelle) 4:501-511.

Barnhart EL, Lee KC, Keren K, Mogilner A, Theriot JA. 2011. An adhesion-dependent switch between mechanisms that determine motile cell shape. PLoS Biol 9:e1001059.

Belvindrah R, Graus-Porta D, Goebbels S, Nave KA, Muller U. 2007. Beta1 integrins in radial glia but not in migrating neurons are essential for the formation of cell layers in the cerebral cortex. J Neurosci 27:13854-65.

Blandin AF, Noulet F, Renner G, Mercier MC, Choulier L, Vauchelles R, Ronde P, Carreiras F, Etienne-Selloum N, Vereb G and others. 2016. Glioma cell dispersion is driven by alpha5 integrin-mediated cell-matrix and cell-cell interactions. Cancer Lett 376:328-38.

Carbonell WS, Murase S, Horwitz AF, Mandell JW. 2005. Migration of perilesional microglia after focal brain injury and modulation by CC chemokine receptor 5: an in situ time-lapse confocal imaging study. J Neurosci 25:7040-7.

Casano AM, Peri F. 2015. Microglia: multitasking specialists of the brain. Dev Cell 32:469-77.

Costa P, Scales TM, Ivaska J, Parsons M. 2013. Integrin-specific control of focal adhesion kinase and RhoA regulates membrane protrusion and invasion. PLoS One 8:e74659.

Cukierman E, Pankov R, Stevens DR, Yamada KM. 2001. Taking cell-matrix adhesions to the third dimension. Science 294:1708-12.

Dalmau I, Vela JM, Gonzalez B, Castellano B. 1997. Expression of LFA-1alpha and ICAM-1 in the developing rat brain: a potential mechanism for the recruitment of microglial cell precursors. Brain Res Dev Brain Res 103:163-70.

De Gasperi R, Gama Sosa MA, Elder GA. 2012. Presenilin-1 regulates the constitutive turnover of the fibronectin matrix in endothelial cells. BMC Biochem 13:28.

Doyle AD, Yamada KM. 2016. Mechanosensing via cell-matrix adhesions in 3D microenvironments. Exp Cell Res 343:60-6.

Dudvarski Stankovic N, Teodorczyk M, Ploen R, Zipp F, Schmidt MH. 2016. Microglia-blood vessel interactions: a double-edged sword in brain pathologies. Acta Neuropathol 131:347-63.

Eyo UB, Dailey ME. 2013. Microglia: key elements in neural development, plasticity, and pathology. J Neuroimmune Pharmacol 8:494-509.

Eyo UB, Miner SA, Weiner JA, Dailey ME. 2016. Developmental changes in microglial mobilization are independent of apoptosis in the neonatal mouse hippocampus. Brain Behav Immun 55:49-59.

Eyo UB, Peng J, Swiatkowski P, Mukherjee A, Bispo A, Wu LJ. 2014. Neuronal hyperactivity recruits microglial processes via neuronal NMDA receptors and microglial P2Y12 receptors after status epilepticus. J Neurosci 34:10528-40.

Finlay BL, Darlington RB. 1995. Linked regularities in the development and evolution of mammalian brains. Science 268:1578-84.

Fraley SI, Feng Y, Krishnamurthy R, Kim DH, Celedon A, Longmore GD, Wirtz D. 2010. A distinctive role for focal adhesion proteins in three-dimensional cell motility. Nat Cell Biol 12:598-604.

Frost JL, Schafer DP. 2016. Microglia: Architects of the Developing Nervous System. Trends Cell Biol 26:587-97.

Ginhoux F, Greter M, Leboeuf M, Nandi S, See P, Gokhan S, Mehler MF, Conway SJ, Ng LG, Stanley ER and others. 2010. Fate mapping analysis reveals that adult microglia derive from primitive macrophages. Science 330:841-5.

Gorelik R, Gautreau A. 2015. The Arp2/3 inhibitory protein arpin induces cell turning by pausing cell migration. Cytoskeleton (Hoboken) 72:362-71.

Graupera M, Guillermet-Guibert J, Foukas LC, Phng LK, Cain RJ, Salpekar A, Pearce W, Meek S, Millan J, Cutillas PR and others. 2008. Angiogenesis selectively requires the p110alpha isoform of PI3K to control endothelial cell migration. Nature 453:662-6.

Greig LC, Woodworth MB, Galazo MJ, Padmanabhan H, Macklis JD. 2013. Molecular logic of neocortical projection neuron specification, development and diversity. Nat Rev Neurosci 14:755-69.

Grinberg YY, Milton JG, Kraig RP. 2011. Spreading depression sends microglia on Levy flights. PLoS One 6:e19294.

Grossmann R, Stence N, Carr J, Fuller L, Waite M, Dailey ME. 2002. Juxtavascular microglia migrate along brain microvessels following activation during early postnatal development. Glia 37:229-40.

Hynes RO. 2002. Integrins: bidirectional, allosteric signaling machines. Cell 110:673-87.

Jung S, Aliberti J, Graemmel P, Sunshine MJ, Kreutzberg GW, Sher A, Littman DR. 2000. Analysis of fractalkine receptor CX(3)CR1 function by targeted deletion and green fluorescent protein reporter gene insertion. Mol Cell Biol 20:4106-14.

Kasahara Y, Koyama R, Ikegaya Y. 2016. Depth and time-dependent heterogeneity of microglia in mouse hippocampal slice cultures. Neurosci Res 111:64-9.

Kierdorf K, Erny D, Goldmann T, Sander V, Schulz C, Perdiguero EG, Wieghofer P, Heinrich A, Riemke P, Holscher C and others. 2013. Microglia emerge from erythromyeloid precursors via Pu.1- and Irf8-dependent pathways. Nat Neurosci 16:273-80.

Kim C, Cho ED, Kim HK, You S, Lee HJ, Hwang D, Lee SJ. 2014. beta1-integrin-dependent migration of microglia in response to neuron-released alpha-synuclein. Exp Mol Med 46:e91.

Lau LW, Cua R, Keough MB, Haylock-Jacobs S, Yong VW. 2013. Pathophysiology of the brain extracellular matrix: a new target for remyelination. Nat Rev Neurosci 14:722-9.

Legate KR, Takahashi S, Bonakdar N, Fabry B, Boettiger D, Zent R, Fassler R. 2011. Integrin adhesion and force coupling are independently regulated by localized PtdIns(4,5)2 synthesis. EMBO J 30:4539-53.

Li C, Zhen G, Chai Y, Xie L, Crane JL, Farber E, Farber CR, Luo X, Gao P, Cao X and others. 2016. RhoA determines lineage fate of mesenchymal stem cells by modulating CTGF-VEGF complex in extracellular matrix. Nat Commun 7:11455.

Lock JG, Wehrle-Haller B, Stromblad S. 2008. Cell-matrix adhesion complexes: master control machinery of cell migration. Semin Cancer Biol 18:65-76.

Madadizadeh F, Ezati Asar M, Hosseini M. 2015. Common Statistical Mistakes in Descriptive Statistics Reports of Normal and Non-Normal Variables in Biomedical Sciences Research. Iran J Public Health 44:1557-8.

Maecker HT, Trotter J. 2006. Flow cytometry controls, instrument setup, and the determination of positivity. Cytometry A 69:1037-42.

Marchetti G, Escuin S, van der Flier A, De Arcangelis A, Hynes RO, Georges-Labouesse E. 2010. Integrin alpha5beta1 is necessary for regulation of radial migration of cortical neurons during mouse brain development. Eur J Neurosci 31:399-409.

Meijering E, Dzyubachyk O, Smal I. 2012. Methods for cell and particle tracking. Methods Enzymol 504:183-200.

Milner R. 2009. Microglial expression of alphavbeta3 and alphavbeta5 integrins is regulated by cytokines and the extracellular matrix: beta5 integrin null microglia show no defects in adhesion or MMP-9 expression on vitronectin. Glia 57:714-23.

Milner R, Campbell IL. 2002a. Cytokines regulate microglial adhesion to laminin and astrocyte extracellular matrix via protein kinase C-dependent activation of the alpha6beta1 integrin. J Neurosci 22:1562-72.
Milner R, Campbell IL. 2002b. Developmental regulation of beta1 integrins during angiogenesis in the central nervous system. Mol Cell Neurosci 20:616-26.
Milner R, Campbell IL. 2002c. The integrin family of cell adhesion molecules has multiple functions within the CNS. J Neurosci Res 69:286-91.
Milner R, Campbell IL. 2003. The extracellular matrix and cytokines regulate microglial integrin expression and activation. J Immunol 170:3850-8.
Milner R, Crocker SJ, Hung S, Wang X, Frausto RF, del Zoppo GJ. 2007. Fibronectin- and vitronectin-induced microglial activation and matrix metalloproteinase-9 expression is mediated by integrins alpha5beta1 and alphavbeta5. J Immunol 178:8158-67.
Moroi M, Onitsuka I, Imaizumi T, Jung SM. 2000. Involvement of activated integrin alpha2beta1 in the firm adhesion of platelets onto a surface of immobilized collagen under flow conditions. Thromb Haemost 83:769-76.
Nasu-Tada K, Koizumi S, Inoue K. 2005. Involvement of beta1 integrin in microglial chemotaxis and proliferation on fibronectin: different regulations by ADP through PKA. Glia 52:98-107.
Nimmerjahn A, Kirchhoff F, Helmchen F. 2005. Resting microglial cells are highly dynamic surveillants of brain parenchyma in vivo. Science 308:1314-8.
Petersen MA, Dailey ME. 2004. Diverse microglial motility behaviors during clearance of dead cells in hippocampal slices. Glia 46:195-206.
Pont-Lezica L, Bechade C, Belarif-Cantaut Y, Pascual O, Bessis A. 2011. Physiological roles of microglia during development. J Neurochem 119:901-8.
Rezaie P, Cairns NJ, Male DK. 1997. Expression of adhesion molecules on human fetal cerebral vessels: relationship to microglial colonisation during development. Brain Res Dev Brain Res 104:175-89.
Rigato C, Buckinx R, Le-Corronc H, Rigo JM, Legendre P. 2011. Pattern of invasion of the embryonic mouse spinal cord by microglial cells at the time of the onset of functional neuronal networks. Glia 59:675-95.
Romberger DJ. 1997. Fibronectin. Int J Biochem Cell Biol 29:939-43.
Ruoslahti E. 1996. Brain extracellular matrix. Glycobiology 6:489-92.
Sauvageot CM, Stiles CD. 2002. Molecular mechanisms controlling cortical gliogenesis. Curr Opin Neurobiol 12:244-9.
Schiefer J, Kampe K, Dodt HU, Zieglgansberger W, Kreutzberg GW. 1999. Microglial motility in the rat facial nucleus following peripheral axotomy. J Neurocytol 28:439-53.
Schmid RS, Anton ES. 2003. Role of integrins in the development of the cerebral cortex. Cereb Cortex 13:219-24.
Sheppard AM, Brunstrom JE, Thornton TN, Gerfen RW, Broekelmann TJ, McDonald JA, Pearlman AL. 1995. Neuronal production of fibronectin in the cerebral cortex during migration and layer formation is unique to specific cortical domains. Dev Biol 172:504-18.
Sheppard AM, Hamilton SK, Pearlman AL. 1991. Changes in the distribution of extracellular matrix components accompany early morphogenetic events of mammalian cortical development. J Neurosci 11:3928-42.
Sieger D, Moritz C, Ziegenhals T, Prykhozhij S, Peri F. 2012. Long-range Ca2+ waves transmit brain-damage signals to microglia. Dev Cell 22:1138-48.
Smolders S, Smolders SM, Swinnen N, Gartner A, Rigo JM, Legendre P, Brone B. 2015. Maternal immune activation evoked by polyinosinic:polycytidylic acid does not evoke microglial cell activation in the embryo. Front Cell Neurosci 9:301.
Stettler EM, Galileo DS. 2004. Radial glia produce and align the ligand fibronectin during neuronal migration in the developing chick brain. J Comp Neurol 468:441-51.
Stewart GR, Pearlman AL. 1987. Fibronectin-like immunoreactivity in the developing cerebral cortex. J Neurosci 7:3325-33.

Svahn AJ, Graeber MB, Ellett F, Lieschke GJ, Rinkwitz S, Bennett MR, Becker TS. 2013. Development of ramified microglia from early macrophages in the zebrafish optic tectum. Dev Neurobiol 73:60-71.

Swinnen N, Smolders S, Avila A, Notelaers K, Paesen R, Ameloot M, Brone B, Legendre P, Rigo JM. 2013. Complex invasion pattern of the cerebral cortex bymicroglial cells during development of the mouse embryo. Glia 61:150-63.

Tanzer ML. 2006. Current concepts of extracellular matrix. J Orthop Sci 11:326-31.

Toyjanova J, Flores-Cortez E, Reichner JS, Franck C. 2015. Matrix confinement plays a pivotal role in regulating neutrophil-generated tractions, speed, and integrin utilization. J Biol Chem 290:3752-63.

Ueno M, Yamashita T. 2014. Bidirectional tuning of microglia in the developing brain: from neurogenesis to neural circuit formation. Curr Opin Neurobiol 27:8-15.

Vicente-Manzanares M, Horwitz AR. 2011. Cell migration: an overview. Methods Mol Biol 769:1-24.

Welser-Alves JV, Boroujerdi A, Tigges U, Milner R. 2011. Microglia use multiple mechanisms to mediate interactions with vitronectin; non-essential roles for the highly-expressed alphavbeta3 and alphavbeta5 integrins. J Neuroinflammation 8:157.

Yao H, Duan M, Yang L, Buch S. 2013. Nonmuscle myosin light-chain kinase mediates microglial migration induced by HIV Tat: involvement of beta1 integrins. FASEB J 27:1532-48.

Yokota Y, Gashghaei HT, Han C, Watson H, Campbell KJ, Anton ES. 2007. Radial glial dependent and independent dynamics of interneuronal migration in the developing cerebral cortex. PLoS One 2:e794.

Yoshida N, Hishiyama S, Yamaguchi M, Hashiguchi M, Miyamoto Y, Kaminogawa S, Hisatsune T. 2003. Decrease in expression of alpha 5 beta 1 integrin during neuronal differentiation of cortical progenitor cells. Exp Cell Res 287:262-71.

Yuryev M, Pellegrino C, Jokinen V, Andriichuk L, Khirug S, Khiroug L, Rivera C. 2015. In vivo Calcium Imaging of Evoked Calcium Waves in the Embryonic Cortex. Front Cell Neurosci 9:500.

Zent RP, A. (Eds.). 2010. Cell-Extracellular Matrix Interactions in Cancer: Springer. 314 p.

Zhang F, Nance E, Alnasser Y, Kannan R, Kannan S. 2016. Microglial migration and interactions with dendrimer nanoparticles are altered in the presence of neuroinflammation. J Neuroinflammation 13:65.

Zhao H, Jiang Y, Cao Q, Hou Y, Wang C. 2012. Role of integrin switch and transforming growth factor Beta 3 in hypoxia-induced invasion inhibition of human extravillous trophoblast cells. Biol Reprod 87:47.

6) Figure Legends

Fig. 1. Microglial migration is developmentally regulated. Microglia movement was recorded in acute brain slices during 6 h using 2-photon time-lapse imaging and cell somas were manually tracked. **(A)** Representative microglial migration tracks in different colors at E13.5 (left panel), E15.5 (middle panel) and E17.5 (right panel) (eGFP/microglia, green). The meninges is located at the top of the image and the ventricle at the bottom (not visible at E15.5 and E17.5). **(B)** Microglial average migration speed $v_{av.}$ (μm/h) decreased significantly over development (Kruskal-Wallis with Dunn's, E17.5 vs E13.5 and E15.5, $P<0.001$). **(C)** Cumulative probability plots of migration speed with matching colors for the ages in (B). E17.5 migration speed distribution shows a shift to lower average speeds. **(D)** The percentage of immobile microglia significantly rose from E13.5 to E17.5 (Kruskal-Wallis with Dunn's, $P=0.014$). Sample size (A-C) as n=cells /N=slices/M=mothers at E13.5: 160/18/12; E15.5: 170/10/8; E17.5: 341/14/9. n (cells) was used as sample size in statistical tests. Sample size (D) as N=slices/M=mothers at E13.5: 18/12; E15.5: 10/8; E17.5: 14/9. N (slices) was used as sample size in statistical tests. Scale bar=100 μm.

Fig. 2. Microglial migration behavior. Experimental set-up see Fig. 1. **(A)** Z-projections (30 μm) of representative time-lapse sequences showing characteristic microglial jumping behavior during migration at E13.5. The microglial soma (arrowheads) translocates in jumps. They first scan their environment (=idling, frames with red arrowheads) by sending out and retracting multiple processes and then migrate in the direction of one process (indicated by yellow arrows). The cell soma then displaces in the direction of that process (=active migration, frames with blue arrowheads) followed by a stationary phase during which the cells explores its environment again (=idling, frames with red arrowheads). The action of the cell towards the next time frame (interval=10min) determines the color of the arrowhead. Zoom-ins see Suppl. Fig. 1. **(B)** Representative instantaneous velocity in function of time plots of a cell migrating at high (left panel), intermediate (middle panel) and low (right panel) speed. Plots show phases of active migration interspersed with idling, defined as an instantaneous speed lower than the threshold of 0.8 μm/min (dotted line). **(C)** Relative idling time

increased significantly over development (Kruskal-Wallis, E17.5 vs E13.5 and E15.5, *P*=0.004 and *P*<0.001). **(D)** Instantaneous speed of the active migration events ($v_{inst.\ act.}$) decreased over development (Kruskal-Wallis, E15.5 vs E15.5, *P*<0.001). **(E)** Cumulative probability plots of the data presented in (D) showing a shift to lower instantaneous speeds at E17.5. Sample size (C) as n=cells/N=slices/M=mothers at E13.5: 150/18/12; E15.5: 170/10/8; E17.5: 349/14/9. n (cells) was used as sample size in statistical tests. Sample size (D) as n=steps from cells in (C) at E13.5: n=832; E15.5: n=972; E17.5: n=1740. n (steps) was used as sample size in statistical tests. Scale bar=30 µm.

Fig. 3. Cortical fibronectin and fibronectin receptor on microglia decrease over development. (A) E13.5 (a1-4), E15.5 (b1-4), E17.5 (c1-4) coronal brain sections (DAPI, blue) with insets zooming in on the cortex (a2, b2, c2), indicating ROIs for analysis (white dotted lines in a3, b3, c3) and fibronectin staining (red, a4, b4, c4). Fibronectin was detectable as dense aggregates at E13.5 and with lower density at E15.5 and E17.5. **(B)** Mean grey value (MGV, 0-255) quantifications of the fibronectin immunostainings in the cortical areas marked in a3, b3 and c3. Fibronectin presence was significantly higher at E13.5 than at E15.5 (*P*=0.041) and E17.5 (*P*<0.001), while presence at E15.5 was significantly higher than at E17.5 (*P*<0.001) (Kruskal-Wallis with Dunn's). **(C)** Representative western blotting for fibronectin deposition in the cortex at E13.5, E15.5 and E17.5 with β-actin as loading control. **(D)** Fibronectin western blotting quantification relative to β-actin. Fibronectin deposition was significantly higher at E13.5 compared to E17.5 (*P*<0.001), while deposition at E15.5 was significantly higher compared to E17.5 (*P*=0.001) (ANOVA with Tukey HSD on log10 transformed data). **(E)** Laser scanning microscopy images (Z-projections) showing E13.5 cortex (e1) with microglia (eGFP, green, e2), nuclear staining (DAPI, blue), fibronectin (greys, e3) and blood vessels (GS-IB_4, red, e4). Microglia are frequently observed in the vicinity of blood vessels (inset zoom) and blood vessels show high fibronectin reactivity (e5, yellow arrowheads in e1). **(F)** Flow cytometry gating strategy to assess α5 integrin (fibronectin receptor) expression on microglial cells in panels G and H. **(G)** The percentage of α5 positive microglial cells subtly, however significant, decreased from E15.5 to E17.5 (Kruskal-Wallis with Dunn's, *P*<0.001). **(H)** The expression level (median fluorescence intensity, MFI) of the α5

positive population significantly decreased from E13.5 to E15 to E17.5 (ANOVA with Tukey HSD on log10 transformed data, all $P<0.001$). At E13.5 embryos were pooled per 2-3 and at E15.5-E17.5 individual embryos were analyzed. Sample size (B) as n=slices/N=embryos/M=mothers at E13.5: 28/3/3; E15.5: 21/3/3; E17.5: 39/3/2. n (slices) was used as sample size in statistical tests. Sample size (D) as N=embryos/M=mothers at E13.5: 8/3; E15.5: 9/3; E17.5: 9/3. N (embryos) was used as sample size in statistical tests. Sample size (G,H) as N=embryos/M=mothers at E13.5: 8/3; E15.5: 16/3; E17.5: 20/3. N (embryos) was used as sample size in statistical tests. FN, Fibronectin. Scale bar (A)=500 µm in a1, b1, c1; 100 µm in insets (all other panels). Scale bar (E) =50 µm in e1, 20 µm in e5.

Fig. 4. α5β1 integrin is not essential for microglia–blood vessel contact. (A) Time-lapse sequences (30 µm Z-projections) at E17.5 showing microglial cells (eGFP, green) capable to migrate (arrowheads) along the surface of blood vessels (GS-IB_4, red) in control as well as after α5β1 integrin blockage in acute brain slices. Frame interval=10 min. **(B)** Modes of microglia-blood vessel contact: Full soma (left panel), touching with a process (middle panel) and free or no contact (right panel). **(C)** The percentage of microglia that made contact with a blood vessel during time-lapse recordings (3-6 hours after blocking onset) was not significantly different after α5β1 integrin blockage compared to isotype at E13.5 (Student *t*-test, $P=0.813$) nor at E17.5 (Mann-Whitney, $P=0.169$). The percentage of microglia that made contact with a blood vessel rose significantly from E13.5 to E17.5 (Mann-Whitney, $P=0.003$). **(D)** The percentage of time spent per cell on a particular contact was not significantly affected by α5β1 blockage (Mann-Whitney, $P=0.683$; 0.802; 1.000 for % Soma; % Process; % Free at E13.5 and $P=0.173$; 0.343; 0.974 for % Soma; % Process; % Free at E17.5, respectively). Sample size (C) as N=slices/M=mothers at E13.5: 9/7 (Iso) and 7/3 (Ab); E17.5: 10/7 (Iso) and 12/3 (Ab). N (slices) was used as sample size in statistical tests. Sample size (D) as n=cells/N=slices/M=mothers at E13.5: 41/9/7 (Iso) and 33/7/3 (Ab); E17.5: 86/10/7 (Iso) and 82/12/3 (Ab). n (cells) was used as sample size in statistical tests. Scale bar (A,B)= 30 µm.

Fig. 5. α5β1 integrin blockage at E13.5 decreases while at E15.5 and E17.5 it increases microglial migration speed. Microglia movement was recorded in acute brain slices in the presence of an α5β1 blocking antibody or isotype control during 6 h using 2-photon time-lapse imaging. Cell somas were manually tracked. **(A)** Representative microglial (eGFP, greys) migration tracks in different colors at E13.5, E15.5 and E17.5. The meninges is located at the top of the image and the ventricle at the bottom (not visible at E15.5 and E17.5). **(B)** At E13.5 α5β1 integrin blockage significantly diminished microglial migration speed $v_{av.}$ (μm/h) compared to isotype (*P*=0.017) while it caused an increase in migration speed at E15.5 (*P*=0.009) and at E17.5 (*P*<0.001) (all Kruskal-Wallis with Dunn's). The effect of the blocking antibody was significantly different across ages (dotted lines; E13.5 vs. E15.5: *P*<0.001; E13.5 vs. E17.5: *P*<0.001; E15.5 vs. E17.5: *P*=0.001; all Kruskal-Wallis with Dunn's). **(C)** Immobile fractions after α5β1 integrin blockage at E13.5, E15.5 and E17.5 did neither differ significantly from isotype (all ages *P*=1.000), nor from control (E13.5 *P*=1.000; E15.5 *P*=0.525; E17.5 *P*=0.146) (all Kruskal-Wallis with Dunn's). The effect of the blocking antibody did not differ across ages (all ages *P*=1.000; all Kruskal-Wallis with Dunn's). **(D)** Cumulative probability distributions (control in black, isotype in grey and α5β1 Ab in red) of average migration speed data in α5β1 blockage conditions show clear shifts from isotype and control distributions. Sample size as n=cells/N=embryos/M=mothers at E13.5: 135/15/8 (Ab), 128/16/11 (Iso); E15.5: 227/11/6 (Ab), 180/11/7 (Iso); E17.5: 213/11/6 (Ab), 246/10/5 (Iso). n (cells) was used as sample size in statistical tests. For sample size control condition see Fig. 1. Isotypes did not affect normal (control) migration. Scale bar=100 μm.

Fig. 6. α5β1 integrin blockage affects idling and instantaneous speed. Experimental set-up see Fig. 7. **(A)** α5β1 blockage at E13.5 significantly increased relative idling time compared to isotype, while at E15.5 and E17.5 it significantly decreased idling (Kruskal-Wallis with Dunn's, E13.5 *P*=0.013; E15.5 *P*=0.015; E17.5 *P*<0.001). **(B)** Instantaneous speed of the active migration events ($v_{inst.\ act.}$) significantly increased at E17.5 after blockage compared to isotype (Kruskal-Wallis with Dunn's, *P*<0.001). **(C)** Cumulative probability plots (control in black, isotype in grey and α5β1 Ab in red) of the data

presented in (B) at E13.5, E15.5 and E17.5 showing a shift to higher instantaneous speeds at E17.5 after α5β1 blockage. Sample size (A) as n=cells/N=slices/M=mothers at E13.5: 121/15/8 (Ab), 134/16/11 (Iso); E15.5: 228/11/6 (Ab), 178/11/7 (Iso); E17.5: 222/11/6 (Ab), 247/10/5 (Iso). n (cells) was used as sample size in statistical tests. Sample size (B) as n=steps from cells in (C) at E13.5: 605 (Ab), 795 (Iso); E15.5: 1749 (Ab), 1076 (Iso); E17.5: 1399 (Ab), 1338 (Iso). n (steps) was used as sample size in statistical tests. For sample size control condition see Fig. 1. Isotypes did not affect normal (control) idling and instantaneous speed.

Suppl. Fig 1. Microglial morphology changes during saltatory migration in the cortex at E13.5. Zoom-ins from the microglial cell in Fig. 2. Yellow arrows point to the process that is chosen to initiate directive migration. Frame interval=10 min. Scale bar=15 µm.

Suppl. Movie 1. Microglial migration along the developing vasculature at E17.5 after isotype application (see Fig. 4C).

Suppl. Movie 2. Microglial migration along the developing vasculature at E17.5 after α5β1 antibody application (see Fig. 4C).

Suppl. Movie 3. Microglial migration and tracking at E13.5 after α5β1 antibody application (see Fig. 5A). Each cell migration track is indicated with a number and different color.

Suppl. Movie 4. Microglial migration and tracking at E15.5 after isotype application (see Fig. 5A). Each cell migration track is indicated with a number and different color.

Suppl. Movie 5. Microglial migration and tracking at E15.5 after α5β1 antibody application (see Fig. 5A). Each cell migration track is indicated with a number and different color.

Suppl. Movie 6. Microglial migration and tracking at E17.5 after isotype application (see Fig. 5A). Each cell migration track is indicated with a number and different color.

Suppl. Movie 7. Microglial migration and tracking at E17.5 after α5β1 antibody application (see Fig. 5A). Each cell migration track is indicated with a number and different color.

Suppl. Movie 8. Microglial migration and tracking at E17.5 after α5β1 antibody application (see Fig. 5A). Each cell migration track is indicated with a number and different color.

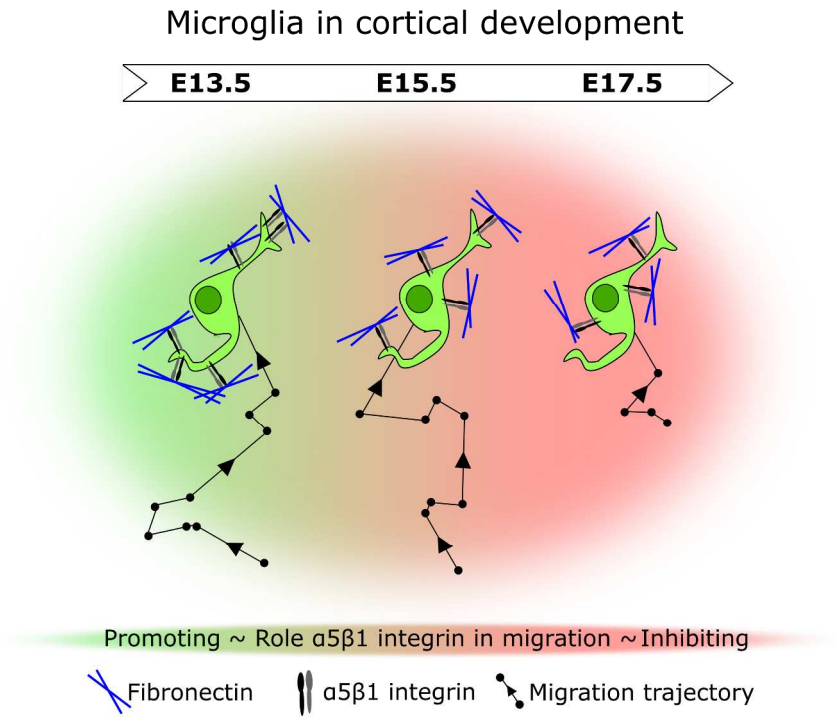

TOCI (Graphical abstract)

209x297mm (300 x 300 DPI)

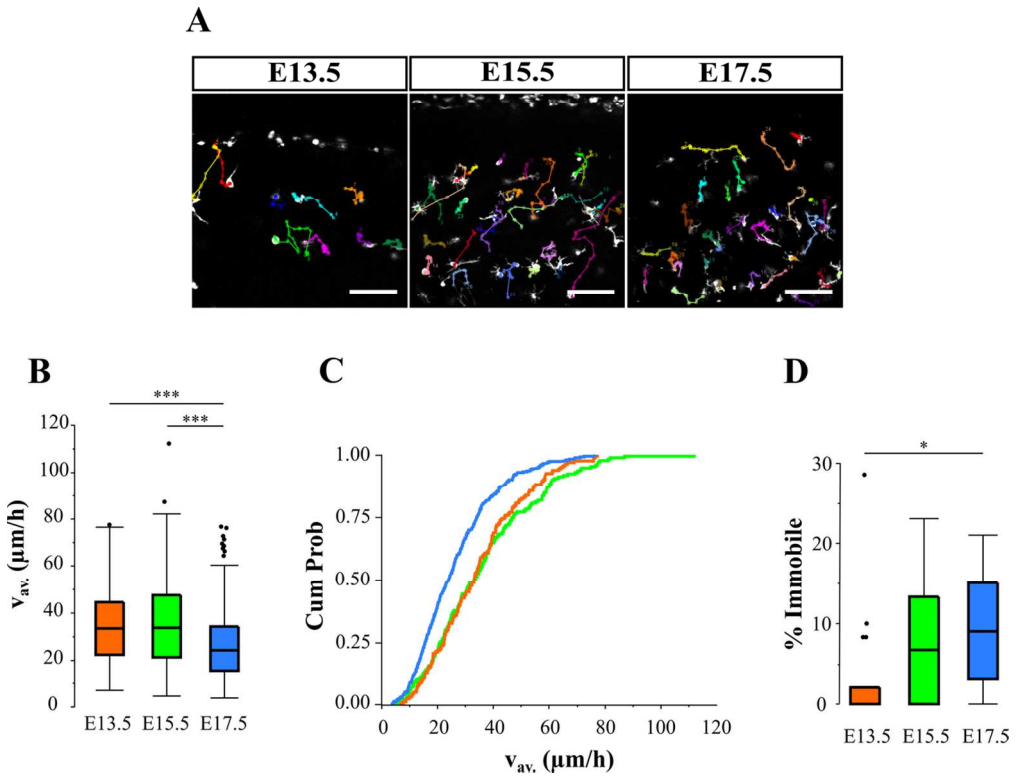

Fig. 1. Microglial migration is developmentally regulated. Microglia movement was recorded in acute brain slices during 6 h using 2-photon time-lapse imaging and cell somas were manually tracked. **(A)** Representative microglial migration tracks in different colors at E13.5 (left panel), E15.5 (middle panel) and E17.5 (right panel) (eGFP/microglia, green). The meninges is located at the top of the image and the ventricle at the bottom (not visible at E15.5 and E17.5). **(B)** Microglial average migration speed vav. (µm/h) decreased significantly over development (Kruskal-Wallis with Dunn's, E17.5 vs E13.5 and E15.5, P<0.001). **(C)** Cumulative probability plots of migration speed with matching colors for the ages in (B). E17.5 migration speed distribution shows a shift to lower average speeds. **(D)** The percentage of immobile microglia significantly rose from E13.5 to E17.5 (Kruskal-Wallis with Dunn's, P=0.014). Sample size (A-C) as n=cells /N=slices/M=mothers at E13.5: 160/18/12; E15.5: 170/10/8; E17.5: 341/14/9. n (cells) was used as sample size in statistical tests. Sample size (D) as N=slices/M=mothers at E13.5: 18/12; E15.5: 10/8; E17.5: 14/9. N (slices) was used as sample size in statistical tests. Scale bar=100 µm.

Fig. 1
120x91mm (300 x 300 DPI)

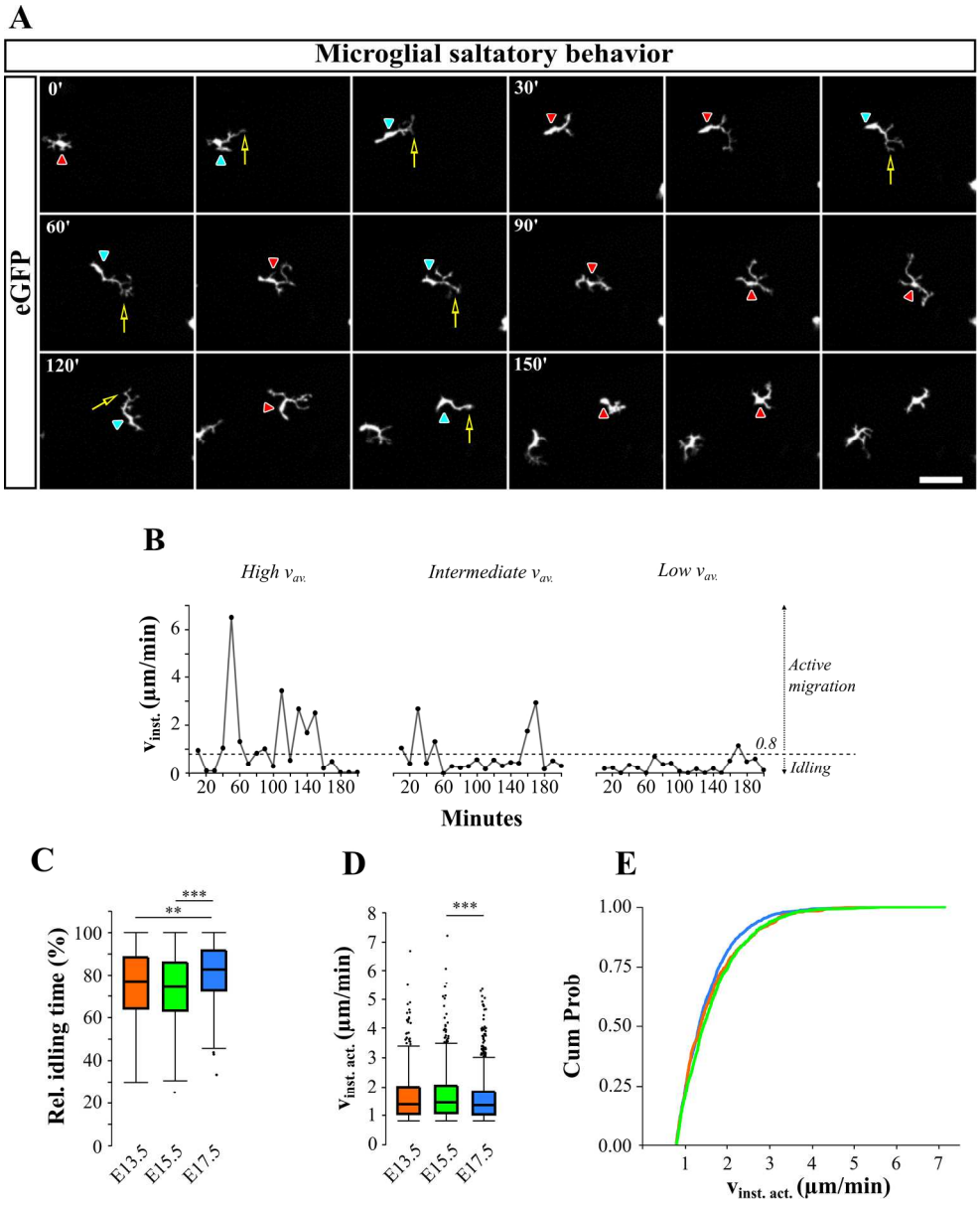

Fig. 2. Microglial migration behavior. Experimental set-up see Fig. 1. **(A)** Z-projections (30 µm) of representative time-lapse sequences showing characteristic microglial jumping behavior during migration at E13.5. The microglial soma (arrowheads) translocates in jumps. They first scan their environment (=idling, frames with red arrowheads) by sending out and retracting multiple processes and then migrate in the direction of one process (indicated by yellow arrows). The cell soma then displaces in the direction of that process (=active migration, frames with blue arrowheads) followed by a stationary phase during which the cells explores its environment again (=idling, frames with red arrowheads). The action of the cell towards the next time frame (interval=10min) determines the color of the arrowhead. Zoom-ins see Suppl. Fig. 1. **(B)** Representative instantaneous velocity in function of time plots of a cell migrating at high (left panel), intermediate (middle panel) and low (right panel) speed. Plots show phases of active migration interspersed with idling, defined as an instantaneous speed lower than the threshold of 0.8 µm/min (dotted line). **(C)** Relative idling time increased significantly over development (Kruskal-Wallis, E17.5 vs E13.5 and E15.5, P=0.004 and P<0.001). **(D)** Instantaneous speed of the active migration events ($v_{inst. act.}$) decreased over

development (Kruskal-Wallis, E15.5 vs E15.5, P<0.001). **(E)** Cumulative probability plots of the data presented in (D) showing a shift to lower instantaneous speeds at E17.5. Sample size (C) as n=cells/N=slices/M=mothers at E13.5: 150/18/12; E15.5: 170/10/8; E17.5: 349/14/9. n (cells) was used as sample size in statistical tests. Sample size (D) as n=steps from cells in (C) at E13.5: n=832; E15.5: n=972; E17.5: n=1740. n (steps) was used as sample size in statistical tests. Scale bar=30 μm.

Fig. 2

197x242mm (300 x 300 DPI)

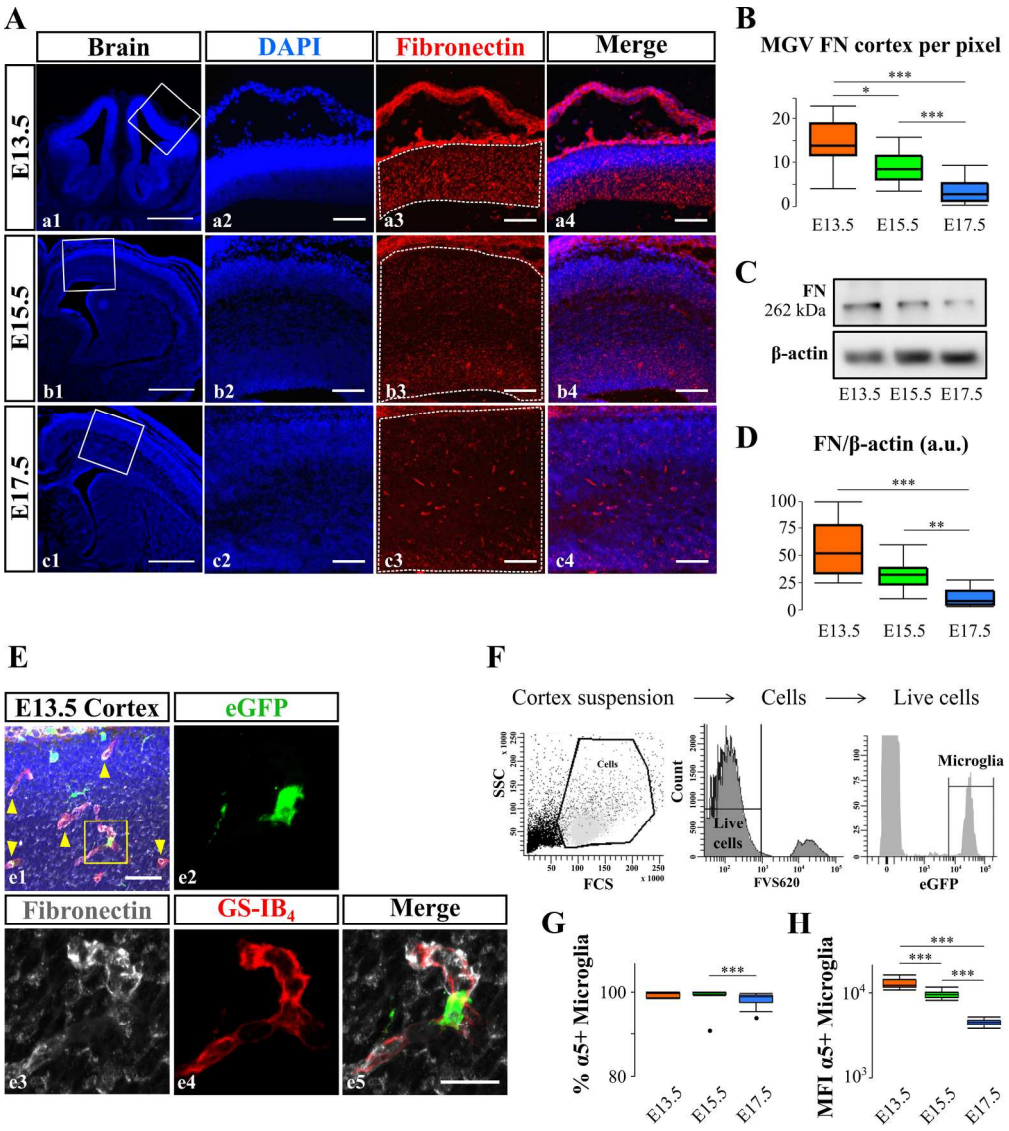

Fig. 3. Cortical fibronectin and fibronectin receptor on microglia decrease over development. (A) E13.5 (a1-4), E15.5 (b1-4), E17.5 (c1-4) coronal brain sections (DAPI, blue) with insets zooming in on the cortex (a2, b2, c2), indicating ROIs for analysis (white dotted lines in a3, b3, c3) and fibronectin staining (red, a4, b4, c4). Fibronectin was detectable as dense aggregates at E13.5 and with lower density at E15.5 and E17.5. **(B)** Mean grey value (MGV, 0-255) quantifications of the fibronectin immunostainings in the cortical areas marked in a3, b3 and c3. Fibronectin presence was significantly higher at E13.5 than at E15.5 ($P=0.041$) and E17.5 ($P<0.001$), while presence at E15.5 was significantly higher than at E17.5 ($P<0.001$) (Kruskal-Wallis with Dunn's). **(C)** Representative western blotting for fibronectin deposition in the cortex at E13.5, E15.5 and E17.5 with β-actin as loading control. **(D)** Fibronectin western blotting quantification relative to β-actin. Fibronectin deposition was significantly higher at E13.5 compared to E17.5 ($P<0.001$), while deposition at E15.5 was significantly higher compared to E17.5 ($P=0.001$) (ANOVA with Tukey HSD on log10 transformed data). **(E)** Laser scanning microscopy images (Z-projections) showing E13.5 cortex (e1) with microglia (eGFP, green, e2), nuclear staining (DAPI, blue), fibronectin (greys, e3) and blood vessels (GS-IB4, red, e4). Microglia are frequently observed in the vicinity of blood vessels (inset zoom) and blood vessels show high fibronectin reactivity (e5, yellow arrowheads in e1). **(F)** Flow cytometry gating strategy to assess α5 integrin (fibronectin receptor) expression on microglial cells in panels G and H. **(G)** The

percentage of α5 positive microglial cells subtly, however significant, decreased from E15.5 to E17.5 (Kruskal-Wallis with Dunn's, P<0.001). **(H)** The expression level (median fluorescence intensity, MFI) of the α5 positive population significantly decreased from E13.5 to E15 to E17.5 (ANOVA with Tukey HSD on log10 transformed data, all P<0.001). At E13.5 embryos were pooled per 2-3 and at E15.5-E17.5 individual embryos were analyzed. Sample size (B) as n=slices/N=embryos/M=mothers at E13.5: 28/3/3; E15.5: 21/3/3; E17.5: 39/3/2. n (slices) was used as sample size in statistical tests. Sample size (D) as N=embryos/M=mothers at E13.5: 8/3; E15.5: 9/3; E17.5: 9/3. N (embryos) was used as sample size in statistical tests. Sample size (G,H) as N=embryos/M=mothers at E13.5: 8/3; E15.5: 16/3; E17.5: 20/3. N (embryos) was used as sample size in statistical tests. FN, Fibronectin. Scale bar (A)=500 μm in a1, b1, c1; 100 μm in insets (all other panels). Scale bar (E) =50 μm in e1, 20 μm in e5.

Fig. 3

196x219mm (300 x 300 DPI)

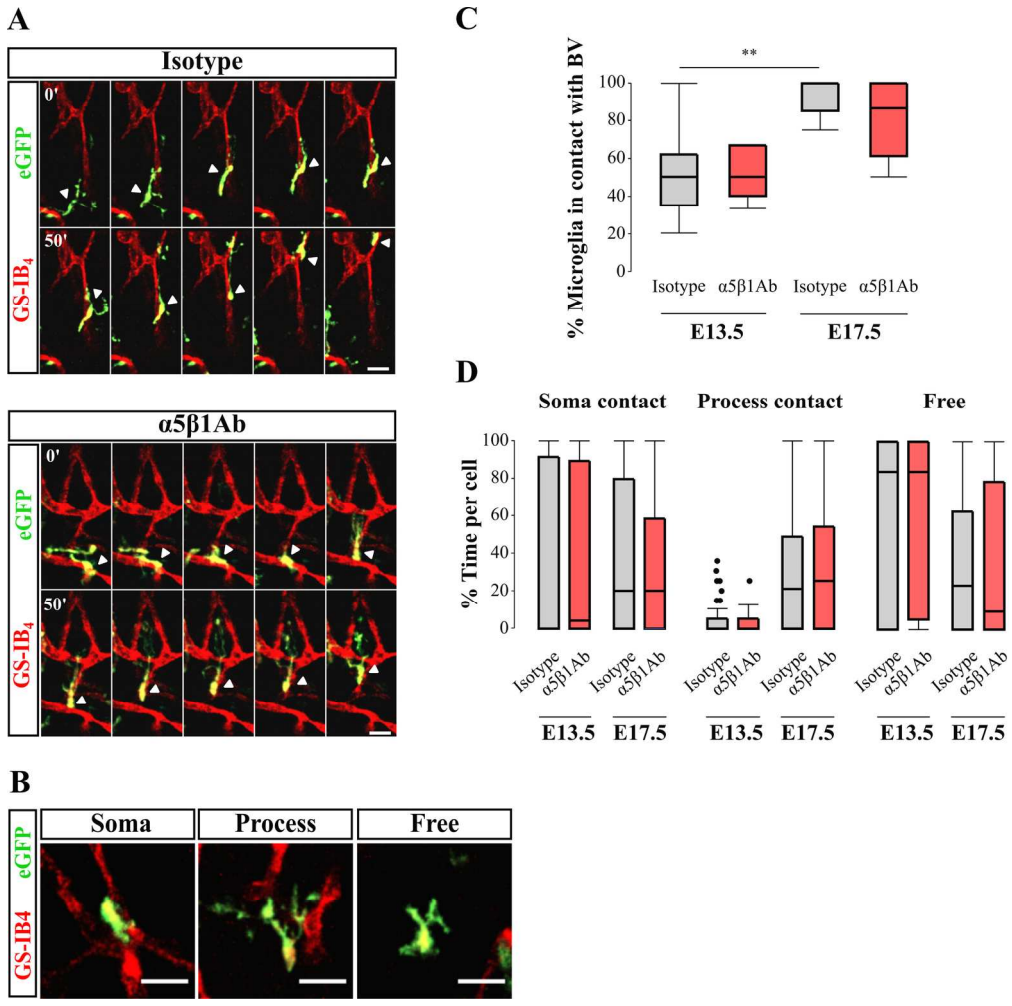

Fig. 4. α5β1 integrin is not essential for microglia–blood vessel contact. (A) Time-lapse sequences (30 µm Z-projections) at E17.5 showing microglial cells (eGFP, green) capable to migrate (arrowheads) along the surface of blood vessels (GS-IB4, red) in control as well as after α5β1 integrin blockage in acute brain slices. Frame interval=10 min. **(B)** Modes of microglia-blood vessel contact: Full soma (left panel), touching with a process (middle panel) and free or no contact (right panel). **(C)** The percentage of microglia that made contact with a blood vessel during time-lapse recordings (3-6 hours after blocking onset) was not significantly different after α5β1 integrin blockage compared to isotype at E13.5 (Student t-test, P=0.813) nor at E17.5 (Mann-Whitney, P=0.169). The percentage of microglia that made contact with a blood vessel rose significantly from E13.5 to E17.5 (Mann- Whitney, P=0.003). **(D)** The percentage of time spent per cell on a particular contact was not significantly affected by α5β1 blockage (Mann-Whitney, P=0.683; 0.802; 1.000 for % Soma; % Process; % Free at E13.5 and P=0.173; 0.343; 0.974 for % Soma; % Process; % Free at E17.5, respectively). Sample size (C) as N=slices/M=mothers at E13.5: 9/7 (Iso) and 7/3 (Ab); E17.5: 10/7 (Iso) and 12/3 (Ab). N (slices) was used as sample size in statistical tests. Sample size (D) as n=cells/N=slices/M=mothers at E13.5: 41/9/7 (Iso) and 33/7/3 (Ab); E17.5: 86/10/7 (Iso) and 82/12/3 (Ab). n (cells) was used as sample size in statistical tests. Scale bar (A, B)= 30 µm.

Fig. 4
173x171mm (300 x 300 DPI)

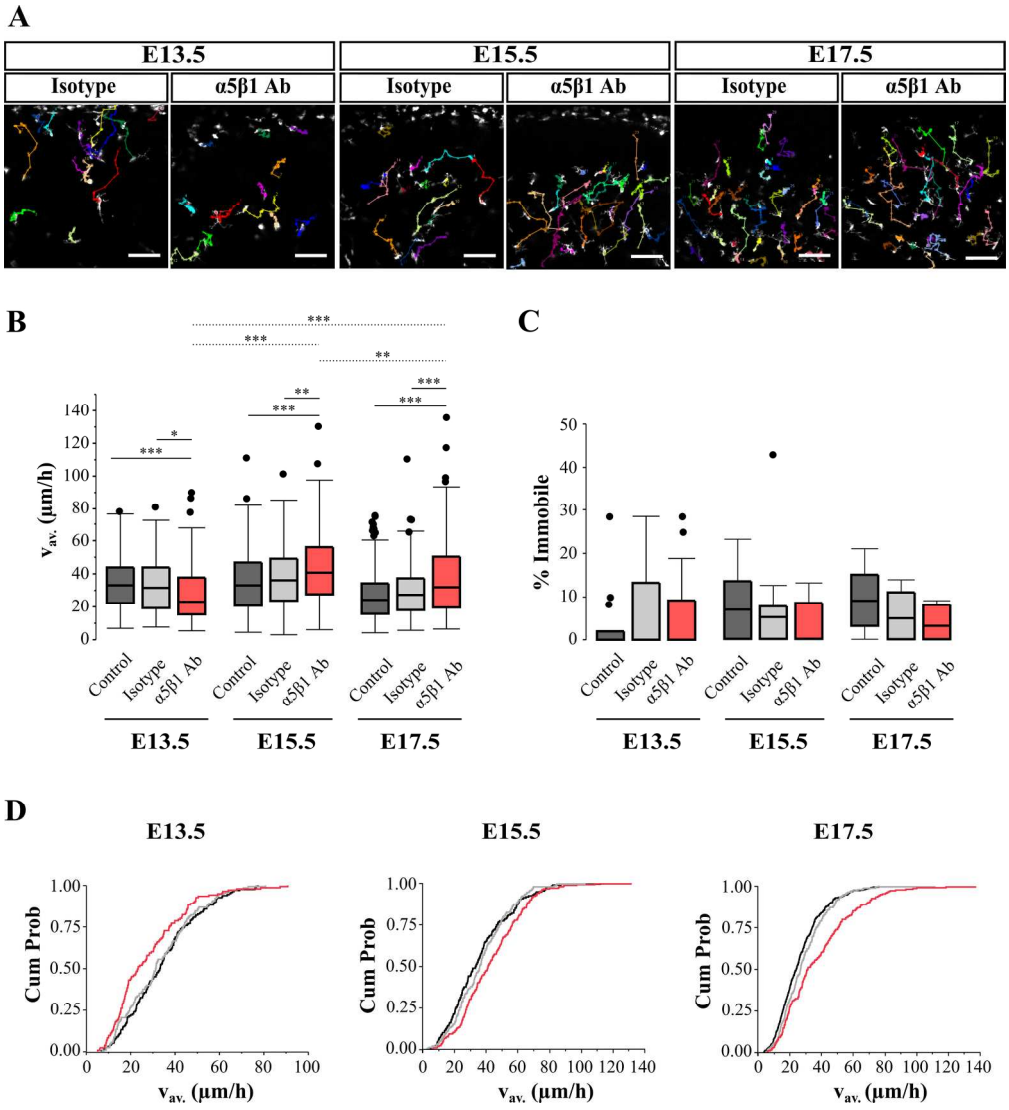

Fig. 5. α5β1 integrin blockage at E13.5 decreases while at E15.5 and E17.5 it increases microglial migration speed. Microglia movement was recorded in acute brain slices in the presence of an α5β1 blocking antibody or isotype control during 6 h using 2-photon time-lapse imaging. Cell somas were manually tracked. **(A)** Representative microglial (eGFP, greys) migration tracks in different colors at E13.5, E15.5 and E17.5. The meninges is located at the top of the image and the ventricle at the bottom (not visible at E15.5 and E17.5). **(B)** At E13.5 α5β1 integrin blockage significantly diminished microglial migration speed $v_{av.}$ (µm/h) compared to isotype (P=0.017) while it caused an increase in migration speed at E15.5 (P=0.009) and at E17.5 (P<0.001) (all Kruskal-Wallis with Dunn's). The effect of the blocking antibody was significantly different across ages (dotted lines; E13.5 vs. E15.5: P<0.001; E13.5 vs. E17.5: P<0.001; E15.5 vs. E17.5: P=0.001; all Kruskal-Wallis with Dunn's). **(C)**Immobile fractions after α5β1 integrin blockage at E13.5, E15.5 and E17.5 did neither differ significantly from isotype (all ages P=1.000), nor from control (E13.5 P=1.000; E15.5 P=0.525; E17.5 P=0.146) (all Kruskal-Wallis with Dunn's). The effect of the blocking antibody did not differ across ages (all ages P=1.000; all Kruskal-Wallis with Dunn's). **(D)**Cumulative probability distributions (control in black, isotype in grey and α5β1 Ab in red) of average migration speed data in α5β1 blockage conditions show clear shifts from isotype and control distributions. Sample size as n=cells/N=embryos/M=mothers at E13.5: 135/15/8 (Ab), 128/16/11 (Iso); E15.5: 227/11/6 (Ab), 180/11/7 (Iso); E17.5: 213/11/6 (Ab), 246/10/5 (Iso). n (cells) was used as sample size in statistical

tests. For sample size control condition see Fig. 1. Isotypes did not affect normal (control) migration. Scale bar=100 μm.

Fig. 5

196x215mm (300 x 300 DPI)

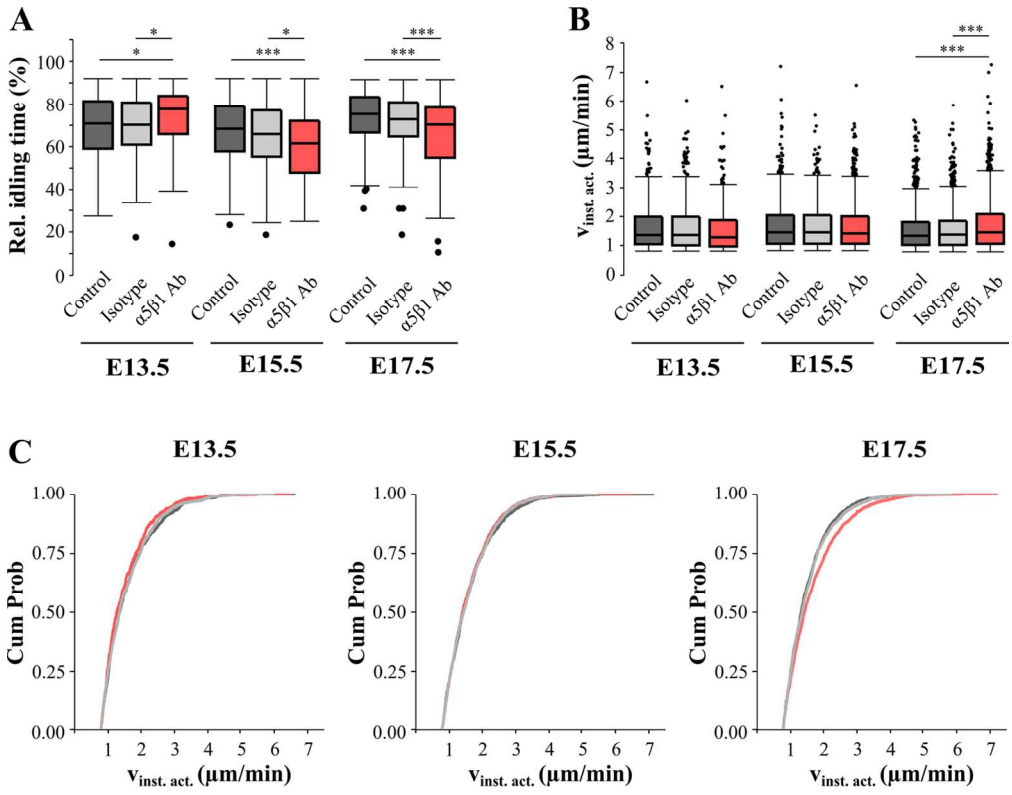

Fig. 6. α5β1 integrin blockage affects idling and instantaneous speed. Experimental set-up see Fig. 7. **(A)** α5β1 blockage at E13.5 significantly increased relative idling time compared to isotype, while at E15.5 and E17.5 it significantly decreased idling (Kruskal-Wallis with Dunn's, E13.5 P=0.013; E15.5 P=0.015; E17.5 P<0.001). **(B)** Instantaneous speed of the active migration events (v**inst. act.**) significantly increased at E17.5 after blockage compared to isotype (Kruskal-Wallis with Dunn's, P<0.001). **(C)** Cumulative probability plots (control in black, isotype in grey and α5β1 Ab in red) of the data presented in (B) at E13.5, E15.5 and E17.5 showing a shift to higher instantaneous speeds at E17.5 after α5β1 blockage. Sample size (A) as n=cells/N=slices/M=mothers at E13.5: 121/15/8 (Ab), 134/16/11 (Iso); E15.5: 228/11/6 (Ab), 178/11/7 (Iso); E17.5: 222/11/6 (Ab), 247/10/5 (Iso). n (cells) was used as sample size in statistical tests. Sample size (B) as n=steps from cells in (C) at E13.5: 605 (Ab), 795 (Iso); E15.5: 1749 (Ab), 1076 (Iso); E17.5: 1399 (Ab), 1338 (Iso). n (steps) was used as sample size in statistical tests. For sample size control condition see Fig. 1. Isotypes did not affect normal (control) idling and instantaneous speed.

Fig. 6
128x100mm (300 x 300 DPI)

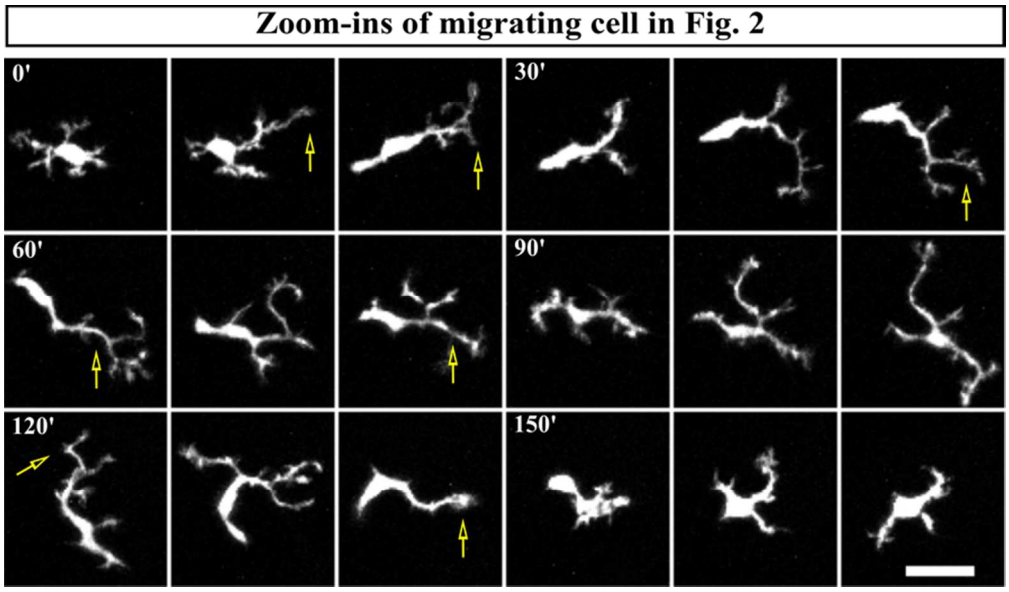

Suppl. Fig 1. Microglial morphology changes during saltatory migration in the cortex at E13.5. Zoom-ins from the microglial cell in Fig. 2. Yellow arrows point to the process that is chosen to initiate directive migration. Frame interval=10 min. Scale bar=15 μm.

Suppl. Fig. 1
75x43mm (300 x 300 DPI)